OH and Soot Optical Diagnostics for Combustion Applications for Combustion Applications

Li, Zheming

2016

Document Version:
Publisher's PDF, also known as Version of record

OH and soot optical diagnostics for combustion applications

Zheming Li

LUND
UNIVERSITY

DOCTORAL DISSERTATION
by due permission of the Faculty of Engineering, Lund University, Sweden.
To be defended at Rydbergsalen, Fysicum, Professorsgatan 1. 13:15 10/14, 2016.

Faculty opponent

Dr. Mark P.B. Musculus

Sandia National Laboratories, Combustion Research Facility, USA

Organization	Document name
LUND UNIVERSITY	Doctoral Dissertation
Division of Combustion Physics Department of Physics P.O Box 118, SE-211 00 Lund, Sweden	Date of issue September 14, 2016
Author(s): Zheming Li	Sponsoring organization

Title and subtitle: OH and soot optical diagnostics for combustion applications

Abstract

Optical diagnostics are remote non-intrusive sensing techniques. The thesis work concerns the use of OH and soot optical diagnostics for combustion research.

Internal combustion (IC) engines are widely used for the generation of power and for transportation purposes. Soot emission, involving carbon particles that emanate from the combustion process, is one of major sources of pollutants in engine exhaust. Such particles can be inhaled into human lungs and have been found to be harmful to public health. For this reason, soot emissions from IC engines are strictly regulated. The flame lift-off length (LOL) of a diesel jet, which is the distance between the nozzle of the injector and the base of the flame, affects both diesel combustion and emission formation. The presence of OH radicals has been used commonly for determining LOL. Both the 2D imaging of OH* chemiluminescence and OH-laser-induced fluorescence (LIF) were employed here for determining the LOL of diesel spray flame. Laser extinction measurements (LEM), together with measurements of the natural luminosity (NL) of sooty flames and of laser-induced incandescence (LII) were made use of for in-cylinder soot detection in the thesis. The main goal in the use of optical diagnostics in engines was to answer various engine-related questions. The optical techniques and the data processing methods employed in the thesis work were also improved parallel to one another. The online/offline OH* chemiluminescence method that was used was able to successfully reduce part of the soot luminosity of the OH* chemiluminescence image obtained. A comparison of LOL results obtained on the basis of simultaneous OH* chemiluminescence and OH-LIF images was carried out. The OH-LIF resulted statistically in longer LOL than the OH*chemiluminescence results did. This can be partially explained by the difference between the two methods in the probing volumes and the flame asymmetry. A data correction for the LEM results was developed, one that helped to reduce the effects of the fluctuations in the probing laser intensities and the soot deposits on the optical window. Simultaneous OH-PLIF and soot-LII was performed for studying the soot oxidation process in the recirculation zone of a diesel optical engine.

In addition to the optical diagnostics applied to the optical engines that were studied, simultaneous dual species PLIF techniques were developed and made use of in the thesis work. Splitting the beam from the multi-YAG laser into two, the one used to pump OPO and the other used directly for formaldehyde (CH2O) excitation, made the simultaneous probing of two species at a high repetition rate possible. Simultaneous OH and CH2O-PLIF was performed for demonstrations at a repetition rate of 50 kHz. The Frequency Recognition Algorithm for Multiple Exposure (FRAME) approach was also introduced. Through the use of structured illumination, FRAME permits several laser-induced signals to be superimposed upon a single detector.

Key words: OH, soot, LIF, LEM, laser diagnostics, optical engine, lift-off length

Classification system and/or index terms (if any)

Supplementary bibliographical information	Language: English
ISSN and key title 1102-8718	ISBN 978-91-7623-973-5
Recipient's notes	Number of pages: 184 / Price
	Security classification

OH and soot optical diagnostics for combustion applications

Doctoral Thesis

ZHEMING LI
(李哲名)

Division of Combustion Physics
Department of Physics

Lund, Sweden
September 2016

LUND
UNIVERSITY

Printed by: Tryckeriet E-husets, Lund, Sweden
September 2016

Lund Reports on Combustion Physics, LRCP-199
ISSN 1102-8718
ISRN LUTFD2/TFCP-199-SE
ISBN 978-91-7623-973-5
Zheming Li
Division of Combustion Physics
Department of Physics
Lund University
P.O. Box 118
SE-221 00, Lund, Sweden

To Mengqin and our children

谨以此书献给我的爱人孟芹以及我的家人们

Abstract

Optical diagnostics are remote non-intrusive sensing techniques. The thesis work concerns the use of OH and soot optical diagnostics for combustion research.

Internal combustion (IC) engines are widely used for the generation of power and for transportation purposes. Soot emission, involving carbon particles that emanate from the combustion process, is one of major sources of pollutants in engine exhaust. Such particles can be inhaled into human lungs and have been found to be harmful to public health. For this reason, soot emissions from IC engines are strictly regulated. The flame lift-off length (LOL) of a diesel jet, which is the distance between the nozzle of the injector and the base of the flame, affects both diesel combustion and emission formation. The presence of OH radicals has been used commonly for determining LOL. Both the 2D imaging of OH* chemiluminescence and OH-laser-induced fluorescence (LIF) were employed here for determining the LOL of diesel spray flame. Laser extinction measurements (LEM), together with measurements of the natural luminosity (NL) of sooty flames and of laser-induced incandescence (LII) were made use of for in-cylinder soot detection in the thesis. The main goal in the use of optical diagnostics in engines was to answer various engine-related questions. The optical techniques and the data processing methods employed in the thesis work were also improved parallel to one another. The online/offline OH* chemiluminescence method that was used was able to successfully reduce part of the soot luminosity of the OH* chemiluminescence image obtained. A comparison of LOL results obtained on the basis of simultaneous OH* chemiluminescence and OH-LIF images was carried out. The OH-LIF resulted statistically in longer LOL than the OH*chemiluminescence results did. This can be partially explained by the difference between the two methods in the probing volumes and the flame asymmetry. A data correction for the LEM results was developed, one that helped to reduce the effects of the fluctuations in the probing laser intensities and the soot deposits on the optical window. Simultaneous OH-PLIF and soot-LII was performed for studying the soot oxidation process in the recirculation zone of a diesel optical engine.

In addition to the optical diagnostics applied to the optical engines that were studied, simultaneous dual species PLIF techniques were developed and made use of in the thesis work. Splitting the beam from the multi-YAG laser into two, the one used to pump OPO and the other used directly for formaldehyde (CH_2O) excitation, made the simultaneous probing of two species at a high repetition rate possible.

Simultaneous OH and CH_2O-PLIF was performed for demonstrations at a repetition rate of 50 kHz. The Frequency Recognition Algorithm for Multiple Exposure (FRAME) approach was also introduced. Through the use of structured illumination, FRAME permits several laser-induced signals to be superimposed upon a single detector.

Popular summary

Man started to use flint knives for making fires in prehistoric times. Thousands of years later, man came to rely in everyday life has high relied on fossil fuel combustion for generating power, for transportations, heating, power plants and the like. Rather recently, exhaust gases produced during the combustion process have been found to lead to global warming. Some of the major combustion products are such air pollutants as soot and nitrogen oxides. Soot is a solid substance consisting mainly of carbon. Soot particles can absorb hydrocarbons and various harmful molecules. The soot emissions produced, which can be inhaled deeply in human lungs, represent a health risk. To reduce the negative effects of soot emissions on public health, many governments have begun to regulate combustion exhaust. A great many studies of combustion have been carried out. The data from conventional measurements alone is not sufficient to efficient understand combustion and further reduce soot emissions. Optical diagnostics play an important role in combustion studies and have done so for decades. Such work has led to the development of different OH and soot optical diagnostic methods for combustion applications.

In contrast to conventional probing measurements, optical diagnostic methods do not disturb the probing medium appreciably when measuring it. They are thus considered to be relatively non-intrusive, and can measure specific species at very low concentrations. They yield results too with a high degree of spatial and/or temporal resolution. Accordingly, optical diagnostics can provide highly detailed information and information of special types for analyzing combustion that more conventional methods are unable to provide.

In the present work, OH laser induced fluorescence (LIF) imaging and OH* chemiluminescence high speed videos were used for visualizing high-temperature flames in part for measuring the flame lift-off length in heavy-duty optical engines. The flame lift-off length is linked to engine soot emissions. Through measuring flame lift-off lengths, an experimental correlation model for the lift-off length with use of different engine parameters could be obtained. This model can be highly useful for predicting the lift-off lengths in future studies.

Laser-induced incandescence (LII) and laser extinction measurements (LEM) were employed in present work for probing in-cylinder soot production. Engine-out soot is usually monitored in conventional experiments. In order to reduce soot emissions,

however, it is not sufficient to simply know how much soot is emitted during combustion. It is also important to understand how and where soot is formed and is burned. Obtaining 2D LII images provides information on soot distribution in the engine, as well as a way of determining where soot is formed and where it is burned. Temporally resolved LEM can measure soot volume fractions as a function of time. Use of LEM in optical engines enables soot formation and burning processes to be analyzed.

There are many other optical diagnostics methods that have been employed in combustion analysis that are not dealt with in the present work. There is much to be done in this area. Through use of optical diagnostics, researchers can obtain a better understanding of combustion generally. Improvement in combustion can result in greater efficiency and lower emissions, which can provide us with a more sustainable and greener world.

List of publications

This thesis is based on the following publications, referred to by their Roman numerals. The papers are appended to the thesis.

I. **Li, Z.,** Yu, X., Lequien, G., Lind , T., Jansons, M., Andersson, Ö. and Richter, M., *Comparison of the Lift-Off Lengths Obtained by Simultaneous OH-LIF and OH* Chemiluminescence Imaging in an Optical Heavy-Duty Diesel Engine*, SAE Technical Paper 2015-24-2418, 2015, doi:10.4271/2015-24-2418.

II. Lequien, G., **Li, Z.,** Andersson, Ö. and Richter, M., *Lift-Off Length in an Optical Heavy-Duty Diesel Engine*, SAE Int. J. Engines 8(2):635-646, 2015, doi:10.4271/2015-01-0793.

III. Lequien, G., **Li, Z.,** Andersson, Ö. and Richter, M., *Lift-Off Length in an Optical Heavy-Duty Diesel Engine: Effects of Swirl and Jet-Jet Interactions*, SAE Int. J. Engines 8(5):2188-2198, 2015, doi:10.4271/2015-24-2442.

IV. **Li, Z.,** Rossel, J., Aldén, M. and Richter, M., *Simultaneous imaging of dual species by Planar Laser Induced Fluorescence at 50 kHz in turbulent premixed flames*, Submitted to Applied Spectroscopy

V. Gallo, Y., **Li, Z.,** Richter, M. and Andersson, Ö., *Parameters Influencing Soot Oxidation Rates in an Optical Diesel Engine*, Accepted by SAE 2016 PFL, 2016-01-2183

VI. **Li, Z.,** Gallo, Y., Lind, T., Andersson, Ö., Aldén, M. and Richter, M., *Comparison of laser-extinction and natural luminosity measurements for soot probing in diesel optical engines*, Accepted by SAE 2016 PFL, 2016-01-2159

VII. Lind, T., **Li, Z.,** Micó, C., Olofsson, N., Bengtsson, P.E., Richter, M. and Andersson, Ö., *Simultaneous PLIF Imaging of OH and PLII Imaging of Soot for Studying the Late-Cycle Soot Oxidation in an Optical Heavy-Duty Diesel Engine*, SAE Int. J. Engines 9(2):2016, doi:10.4271/2016-01-0723.

Related work

A. Ehn, A., Bood, J., **Li, Z.,** Berrocal, E., Aldén, M. and Kristensson, E., *FRAME-a videography method for ultrafast science*, Submitted to Nature

B. Kristensson, E., **Li, Z.,** Berrocal, E., Richter, M. and Aldén, M., *Instantaneous 3D imaging of flame species using coded laser illumination*, Accepted for oral presentation at the 36th International Symposium on Combustion, Seoul 2016

C. **Li, Z.,** Borggren, J., Aldén, M. Richter, M., and Kristensson, E., *Simultaneous multiple species imaging in a flame using FRAME*, In manuscript

D. Rossel, J., Bai, X.S., Sjöholm, J., Zhou, B., **Li, Z.,** Wang, Z., Pettersson, P., Li, Z., Richter, M. and Aldén, M., *Multi-species PLIF study of the structures of turbulent premixed methane/air jet flames in the flamelet and thin-reaction zones regimes*, Submitted to Combustion and Flame

E. Wang, Z., Stamatoglou, P., **Li, Z.,** Aldén, M. and Richter, M., *Simultaneous multi-species visualization of a premixed turbulent jet flame by using ultrahigh speed planar laser induced fluorescence imaging*, In manuscript.

Contents

Abbreviations

NO_x	Nitrogen oxides
OH	Hydroxyl
LIF	Laser-Induced Fluorescence
OPO	Optical Parametric Oscillator
KDP	Potassium di-deuterium phosphate
ICCD	Intensified Charge-Coupled Device
CMOS	Complementary Metal Oxide Semiconductor
UV	Ultraviolet
LUPJ	Lund University Piloted Jet
IC	Internal Combustion
LII	Laser-Induced Incandescence
LEM	Laser Extinction Measurements
LOL	Lift-Off Length
CAD	Crank Angle Degree
CH_2O	Formaldehyde
PAH	Polycyclic Aromatic Hydrocarbons
THG	Third Harmonic Generation
SHG	Second Harmonic Generation
FRAME	Frequency Recognition Algorithm for Multiple Exposures
NL	Natural Luminosity
KL	The mean extinction coefficient along the beam path.
AOM	Acousto-Optic Modulator
PD	Photodiode

PMT	Photomultiplier
RPM	Rounds Per Minute
IR	Infrared

1 Introduction

Combustion has been used as the main power source of the world for more than a century. As shown in Figure 1.1, by 2013 more than 80% of the primary energy supply of the world stemmed from use of fossil fuel. Although the proportion of it obtained from biofuels and waste had increased to 10.2% by 2013 [1], combustion is still the dominant method for generating power.

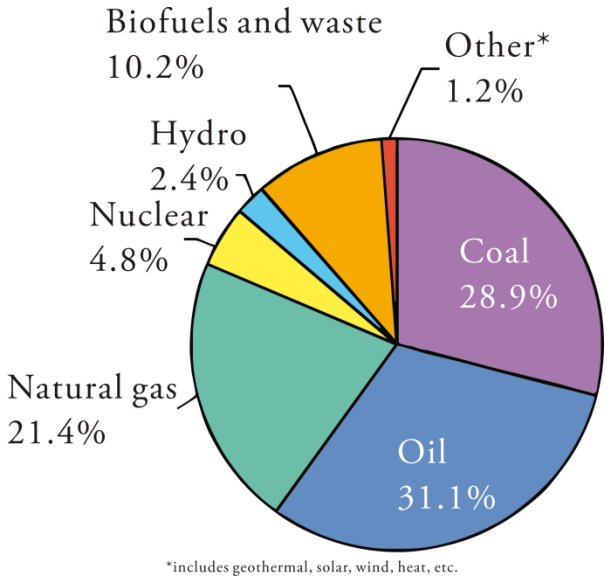

Figure 1.1 Sources of the total primary energy supply in the world by 2013[1].

In the simplified case of hydrocarbon combustion, the products of perfect combustion are water and carbon dioxide. In real combustor or engine combustion, however, it is unavoidable to have incomplete combustion, in which incomplete combustion pollutant species- such as unburned hydrocarbons, carbon monoxide and soot are present in the exhaust. For diesel engines, soot and nitrogen oxides (NO_x) are the two primary pollutants. Nowadays, the emission of global greenhouse gases is increasing. Between 2013 and 2030 the world's economy can be expected to grow by some 88% whereas the aim for the growth of energy-related CO_2 during this period is only 8% [2]. Although the use of renewables can be expected to keep increasing, in

order to achieve this goal it is necessary to improve the efficiency of the combustors and engines that are employed. Questions concerning how a sufficient increase in the efficiency of combustion and a sufficient decrease in the emissions can be achieved are major challenges to researchers.

Optical diagnostics have proven to be powerful tools for the study of combustion phenomena. Multiple dimensional (2D and 3D) information concerning flame intermediates, flow field and temperature can be achieved by use of optical diagnostics. Specific species and radicals can be probed there by use of particular lasers. Laser diagnostics also enables a high degree of temporal and spatial resolution to be achieved. In addition, optical diagnostics are considered to be relatively non-intrusive. Such considerations have led to optical diagnostics being widely used in combustion research. OH radicals, representing one of the most important chemical intermediates in combustion systems, have been studied for decades. 2D laser-induced fluorescence (LIF) imaging of OH, for example, having been employed in the study of flame since the 1980s [3]. Since then, OH-LIF imaging has been developed both in terms of higher repetition rates and multiple dimensional [4-10]. Recently, the time resolved 3D imaging of OH-LIF and OH* chemiluminescence has been reported [11, 12]. Soot, one of the most primary pollutants here, is also one of the particles most commonly studied by use of optical diagnostics. For instance, soot-laser induced incandescence (LII) can provide information concerning soot distribution qualitatively and quantitatively [13, 14]. Laser extinction measurement (LEM) can also provide temporal soot information on regions within the path of laser beam [15]. The information of this sort that optical diagnostics provides can help people improve combustion efficiency and can reduce the amount of pollutants present in the exhaust through increased understanding of the processes involved.

The major aim of the thesis work here is to employ and develop the use of both OH and soot optical diagnostics for combustion research. Chapter 2 describes the major equipment employed. Chapter 3 introduces briefly theories pertaining to the primary methods employed in the thesis. Chapter 4 summarizes both the use of OH diagnostics for studying optical engines and the development of dual-species PLIF imaging techniques that are applicable here. Chapter 5 takes up efforts that have been made to develop in-cylinder soot diagnostics techniques. Various challenges encountered in the course of the experiments and various results of ours in addition to those published in Papers I to VII will be presented both in Chapters 4 and 5. At the end, Chapter 6 provides a brief summary of the thesis and of work that could be envisioned as stemming from it.

2 Experimental equipment

This chapter describes the experimental equipment employed in the thesis work. Certain technical considerations regarding use of the equipment involved will be described briefly.

2.1 Laser systems

Lasers play a major role in optical diagnostics. In the thesis work, use in this respect was made primarily of Nd:YAG lasers, dye lasers, an optical parametric oscillator (OPO) and a diode laser.

Nd:YAG is one of the most commonly employed solid-state lasers. Lasers can be either pulsed or continuous. Pulsed lasers can generally deliver a high level of power within a short period of time, the high laser power making it easier to distinguish the laser-induced signals from the background signals. In the thesis work, pulsed Nd:YAG lasers were used as light sources. They were pumped by flash lamps, the pulse duration being controlled by Q-switches. The laser emission had a wavelength of 1064 nm. Higher frequencies can be generated by frequency doubling and mixing. The laser power can be changed by adjusting the timing of the Q-switch delay relative to the flash-lamp discharge.

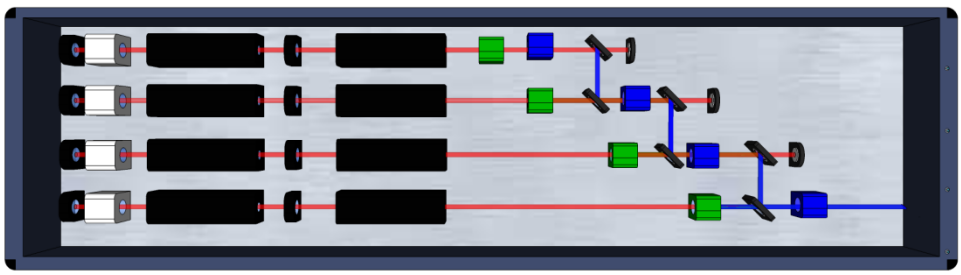

Figure 2.1 Diagram of the multi-YAG laser system in a 355 nm configuration.

Nd:YAG lasers typically work at a 10 Hz repletion rate. High-speed laser systems are required for the diagnostics of rapidly acting events, specifically those taking place in turbulent combustion. Single flash lamp pumped lasers are unable to deliver both a high output power and a high repetition rate. One alternative to use of them is to combine several flash lamp pumped lasers. The Division of Combustion Physics at Lund University has two multi-YAG laser systems, each of them consisting of four individual Nd:YAG lasers in a cluster, each channel of which can Q-switch twice during a single flash-lamp-discharge period, this providing two pulses in a single channel. Such a multi-YAG laser system can emit a train of 8 pulses within a very short period of time. The time separation between two adjacent pulses can be adjusted from 5 to 200 μs. A diagram of the multi-YAG laser system is shown in Figure 2.1. Further information concerning the multi-YAG laser systems can be found in [16-18].

In the thesis work, use was made of both an ordinary 10 Hz Nd:YAG laser (Continuum Powerlite 9010 DLS) and the multi-YAG laser system. The specifications of the two laser systems are shown in Table 2.1.

Table 2.1 The maximum output power of a Continuum Nd:YAG and of the multi-YAG laser systems

Output wavelength	Continuum Nd:YAG laser [mJ/pulse]	Multi-YAG laser	
		Single-pulse mode [mJ/pulse]	Double-pulses mode [mJ/pulse]
1064 nm	2000	1500	700
532 nm	1070	800	350
355 nm	670	320	220
266 nm	210	130	70

Nd:YAG laser emissions are of a single fixed wavelength. Dye lasers and OPO are commonly used together with YAG lasers, their providing a laser output of tunable wavelength. An organic dye solution is used as the gain medium, its producing broadband fluorescence. A grating is employed for selecting the wavelength of the laser output. Laser radiations of differing wavelength can be obtained through use of various dye solutions. The dye solution used in the present work for OH-LIF excitation was Rodanmin 6G. The dye laser was pumped by an Nd:YAG laser at 532 nm. The output wavelength of the laser was tuned to 568 nm, its then being

converted to 284 nm through use of a potassium di-deuterium phosphate (KDP) crystal.

OPO changes the laser wavelength in a different way. It splits a single input photon into two photons with lower frequency. The energy of the photons of lower frequency is dependent upon the angle of the active crystal. The converting efficiency of OPO is slightly lower than that of the dye laser at most wavelength range. The output linewidth of OPO is also broader than that of the dye laser. However, OPO does not suffer from color fading when the pumping laser has a high repetition rate as compared with the dye laser. In the present work, OPO (from GWU) was used for high speed OH-PLIF measurement, whereas the dye laser was used for 10 Hz OH-PLIF. Further information about OPO can be found in [17, 19]. A comparison of OPO with the dye laser here is shown in Table 2.2.

Table 2.2 A comparison of the use of OPO with that of a dye laser

	Dye laser	**OPO**
Wavelength of the pumping laser	532 /355 nm	355 nm
Maximum power of the pumping laser	800 mJ/pulse at 10Hz	160 mJ/pulse at 50 kHz
Linewidth of the output laser	<0.7 cm^{-1}	~4 cm^{-1}
Wavelength range of the output laser	370-760 nm	400-700 nm
Converting efficiency at an output of 568 nm	~25%	~15%

2.2 Detectors

Either charge-coupled device (CCD) or complementary metal-oxide-semiconductor (CMOS) sensors are generally employed in digital cameras. Neither technology has a clear advantage in terms of image quality. However, the readout method used for CCD and CMOS differ, that used for CCD allowing it to be short-gated and that

used for CMOS enabling it to be re-exposed at a high repetition rate. In the thesis, cameras of both types are employed for the different applications involved.

Image intensifiers are add-on devices used in detectors. In combustion diagnostics, intensifiers are commonly employed for two basic reasons, the one being to convert the wavelength of the target signal to a range for which the detector is sensitive, the other being to enhance the distinguishability of the target signal from the background by short-gating and/or by signal amplification. In the thesis, all of the CCDs employed are intensified CCDs. A high speed intensifier (Lambert HS IRO 2 stage) was used together with a high speed CMOS camera for ultraviolet (UV) detection. For further information regarding intensifiers, see reference [20].

Figure 2.2 A photograph of the SIM 8 framing camera.

Two framing cameras - an Imaging SIM 8 camera and a Hadland Imacon 468 camera -were employed so as to be able to match the high repetition rate of the multi-YAG system. The resolutions of these two detectors were 1024x1024 and 512x512, respectively. In both cameras, a fast image intensifier was located directly after the camera's optical entrance so as to enhance the camera's sensitivity and to enable UV detection to take place. The intensified signal was then split into eight sub-images, each of which was relayed to someone of the eight individual intensified CCD modules. A photograph of the SIM 8 camera employed is shown in Figure 2.2. For further details regarding the cameras, see references [16, 17].

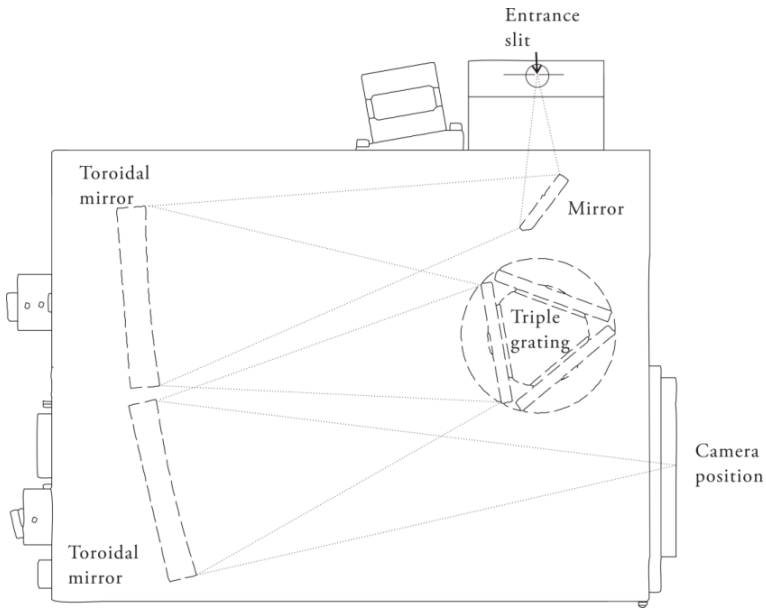

Figure 2.3 A diagram of the Acton 2300i spectrometer

A spectrometer is a spectrographic instrument typically used for obtaining spectrally resolved measurements for recording laser-induced signals or self-radiation spectra in combustion studies. Figure 2.3 is a diagram of the camera-coupled spectrometer (Princeton Instruments, Acton SP-2300i) used in the thesis work. A spectrometer of this type does not by itself measure the wavelength of the signal. It only separates signals of different wavelengths and transmits them to a camera. The wavelength scale needs to be calibrated on the basis of spectral lines of known types, such as mercury lamp spectra.

A photodiode is a semiconductor device that converts light to electric current. In the present study, photodiodes were used for monitoring the timing and the intensity of the lasers employed.

2.3 Combustion equipment

For the development of the optical diagnostics used in the thesis work, various experiments were carried out in a jet burner, the application of the optical diagnostics being performed in an optical engine.

2.3.1 Jet burner

The Lund University Piloted Jet (LUPJ) burner was a modified Mckenna-type burner. The center jet was 1.5 mm in diameter and the pilot flow plug surrounding it was 61 mm in diameter. A photograph of the LUPJ flame upon which a drawing of the cross-section of the burner is superimposed in Figure 2.4.

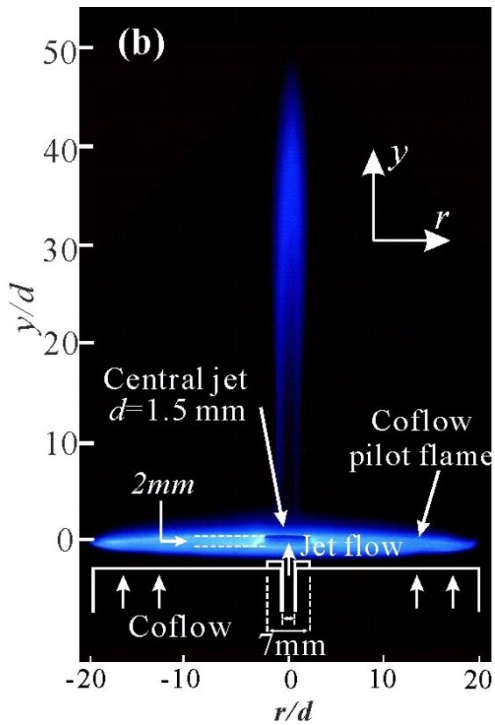

Figure 2.4 A photograph of the LUPJ flame replotted from [21].

In the LUPJ, the central jet flame is surrounded by a hot and reacting flow used to compensate for the heat loss and sustain the flame under high flow velocity conditions. The LUPJ is a good platform to use in performing basic turbulent flame studies. For further information concerning LUPJ, see references [17, 22, 23].

2.3.2 Optical engines

Optical diagnostics are widely used as a means of gaining a better understanding of the combustion process taking place in internal combustion (IC) engines. The optical access involved needs to be one adequately adapted to a metal engine. Optical engines of a Bowditch design are widely used for optical diagnostics [24].

The optical engine employed in the present work was one adapted to use in a Scania D12 heavy-duty diesel engine having an extended piston in one of its cylinders. The extended piston top has been replaced by a piece of quartz used to provide optical access to the combustion chamber. The cylinder head was separated from the cylinder block so as to be able to install an extended piston. A liner having four optical windows was mounted between the cylinder head and the extension block. Photographs of the optical engine are shown in Figure 2.5.

The optical engine of Bowditch design possesses the main features of the original metal engine but provides the possibility of studying the combustion process in a visible way.

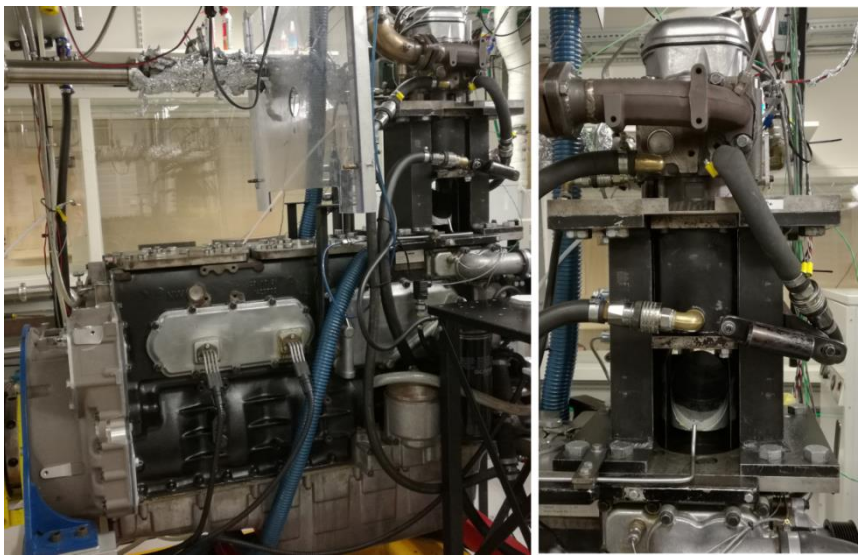

Figure 2.5 Photographs of the optical engine.

2.4 Synchronization of the laser and the camera

During the laser experiments, it was necessary for the camera gate to be locked precisely to the laser pulse in order for it to catch the laser-induced signal. The cameras were usually triggered by a Q-switch pulse operated by the probing laser. One reason for this is that the Q-switching time is very close in length to the laser output time (< 100 ns). The camera was able to easily register a laser-induced signal having a relatively long gate time even without the laser being monitored by a

photodiode. Since the Q-switch out time was close in length to the laser output time, it also provided less jitter than a T_0 or flash-lamp-out to laser-out, this making it possible to use a shorter gate time for the camera. For the laser diagnostics used in the flame measurements carried out, a shorter gate time was required so as to minimize the background signal.

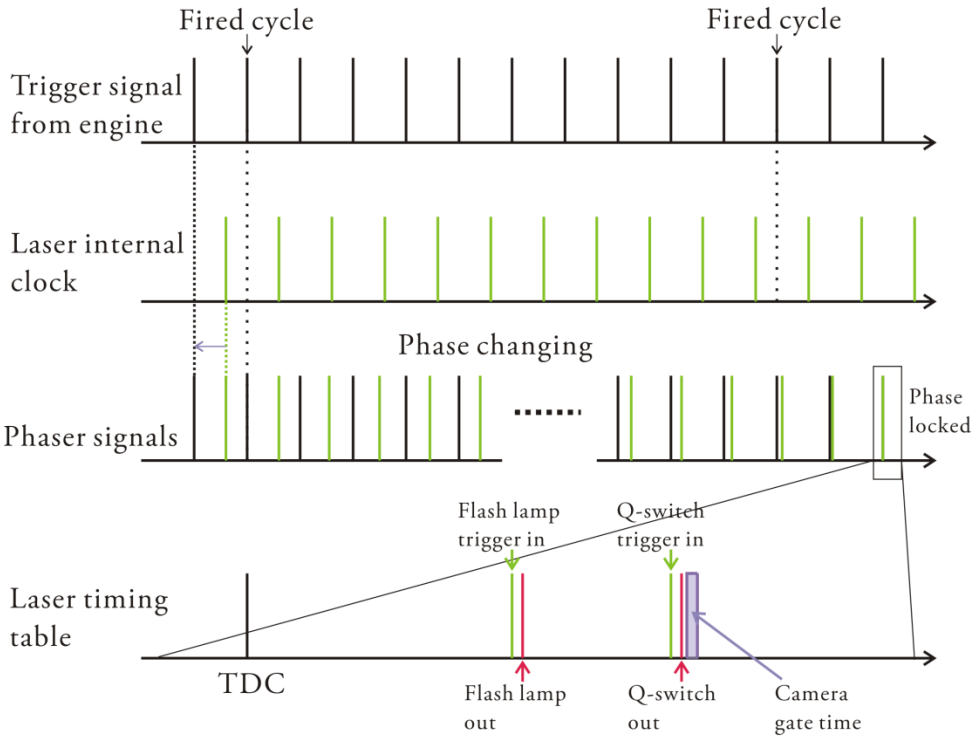

Figure 2.6 Explanation of how the 'phaser' works.

The repetition rate of a normal Nd:YAG laser can only be adjusted to a slight degree due to the inter-lock that occurs. For example, 10 Hz Nd:YAG lasers can work within a range of 9.8 to 10.2 Hz, whereas engines can run anywhere from tens of rounds per minute (RPM) to thousands of RPM. When a four-stroke engine runs at 1200 RPM and if the engine gives a single pulse trigger in each cycle, this generates a 10 Hz pulsed signal. Thus, 1200 RPM or a multiple of it is commonly used for synchronization with a 10 Hz laser. Yet the laser has its own phase at 10 Hz, the engine running in its phase at 10 Hz as well. If the trigger in the source of the laser were switched directly from its internal phase to an engine-out signal, the laser would very likely stop working immediately, since the phasing that occurred would not match with its own phase even though it is also at 10 Hz. A device called a 'phaser'

was made to gradually shift from the engine phase to the laser phase. In measurements of the engine, the laser was started prior to the start of the engine so as to provide stable laser output power. When the engine was stabilized at 1200 RPM, the laser was synchronized with the engine at 10 Hz through the operation of this 'phaser' until the laser phase locked to the engine, as is shown in Figure 2.6. As long as the two phases are locked, the 'phaser' does not change the phase at all.

3 Methods

This chapter provides a brief review of the optical diagnostics techniques used in the thesis. OH* chemiluminescence and flame natural luminosity imaging, will be dealt with first. The section that follows describes the LIF of different species. LII and LEM are also presented in this chapter.

3.1 OH* chemiluminescence

OH is generally formed during high temperature reactions. Thus, the presence of OH radicals is used as a marker of the high temperature reaction region of a flame. In a high temperature environment, the OH that is present exists in two types. For the most part, the OH radical would remain in the ground state, whereas in high temperature regions some of the OH would appear in an excited state. The OH in an excited state is usually marked by a star, OH*, so as to distinguish it from OH in the ground state. The OH* then drops back to the ground state when photons are emitted, the occurrence of this emission being referred to as OH* chemiluminescence.

A spectrum of OH* chemiluminescence is shown in Figure 3.1. As can be seen there are two peaks at 283 and 309 nm, their being due to the excited OH* to the ground state radiation produced [25]. Since the peak at 283 nm is rather small and is difficult to detect, in the present work only the 309 nm peak was taken account of in OH* chemiluminescence measurements.

Since OH* chemiluminescence is in the UV range, which is outside the range that normal camera sensors are sensitive to, it is necessary here to use a UV sensitive intensifier coupled with a camera for OH* chemiluminescence detection. For engine measurements, OH* chemiluminescence in the upstream region of a diesel spray (all up or downstream mentioned in the thesis describes the fuel spray direction) has been found to provide the best marker of the flame lift-off length (LOL) [26, 27]. A band pass filter centered at 310 nm (10 nm FWHM) was used in the thesis work for the subtraction of OH* chemiluminescence from the background signal, as is shown in Figure 3.1.

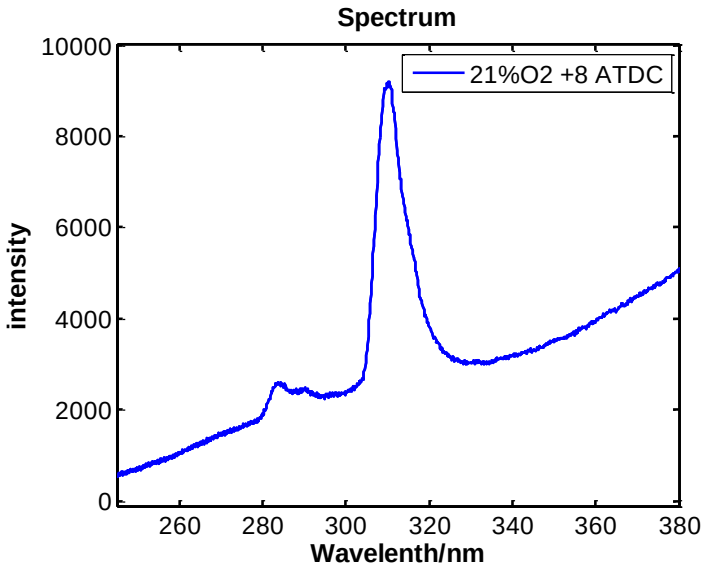

Figure 3.1 The spectrum of an n-heptane diffusion flame in an optical engine.

The OH* chemiluminescence results should normally not be used for quantitative OH analysis. Since the excited state OH* does not represent proportionally the OH radicals of the ground state, the relation of OH* to OH in the ground state depends upon the temperature and on other factors.

3.2 Flame natural luminosity

In Figure 3.1, one can note that, except for the OH* chemiluminescence peak at 309 nm, there is a gradually increasing background signal. This background signal is from the flame natural luminosity. The dominant source of this luminosity is the broadband thermal radiation from hot soot particles during the combustion of traditional hydrocarbon diesel like fuel after premixed burning of it [28].

$$B_\lambda(\lambda, T) = \frac{2hc^2}{\lambda^5} \frac{1}{e^{\frac{hc}{\lambda k_B T}} - 1} \tag{3.1}$$

From Planck's law for blackbody radiation, as given in equation 3.1, where k_B is the Boltzmann constant, h is the Planck constant and c is the speed of light in the medium, the spectral radiance of a body, B_λ , describes the power emitted per unit

area of the body given off as radiation of different wavelength. Equation 3.1 shows B_λ as a function of λ and T. It should be noted that at a given wavelength the intensity of the natural luminosity of soot is linked to the volume of the soot and is also highly sensitive to the temperature.

The flame natural luminosity can be used to measure the soot volume, but only if such matters as the range of the wavelength that is detected and the soot temperature are known.

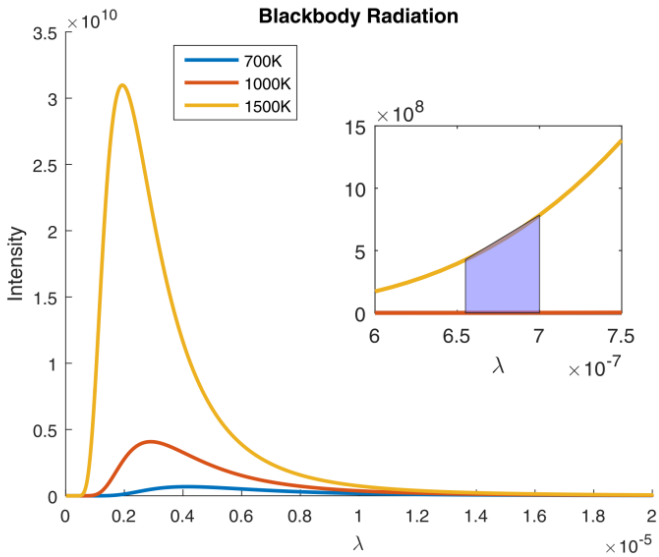

Figure 3.2 Blackbody radiation curves shown for different temperatures as a function of the wavelength.

Figure 3.2 shows three curves of blackbody radiation at different temperatures. The peak position of the curve shifts to shorter wavelengths when the temperature becomes higher. The radiation intensity is generally higher at high than at low temperatures.

In Figure 3.3, the natural luminosity from a diffusion n-heptane flame is plotted as a function of the crank angle degree (CAD). As mentioned above, soot is the dominant source of flame natural luminosity in this case. During the combustion process, the soot temperature is not constant. If data concerning the natural luminosity is used as an indication of the soot volume, the effects of the temperature need to also be considered. In Figure 3.3, the flame natural luminosity is compensated for by the global temperature of the engine. Since both curves have been normalized, it can be seen that in the late cycle after 25 CAD has been passed the T-compensated curve shows the presence of a greater amount of soot than was present in the original curve.

The reason for this is that after 25 CAD the estimated global in-cylinder temperature was found to be less than 800 K under this engine condition. When the amount of soot is the same in both cases, the intensity of the luminosity is much less at 800 K than at 1500 K. Thus after the temperature compensation, the red curve shows more soot after 25 CAD.

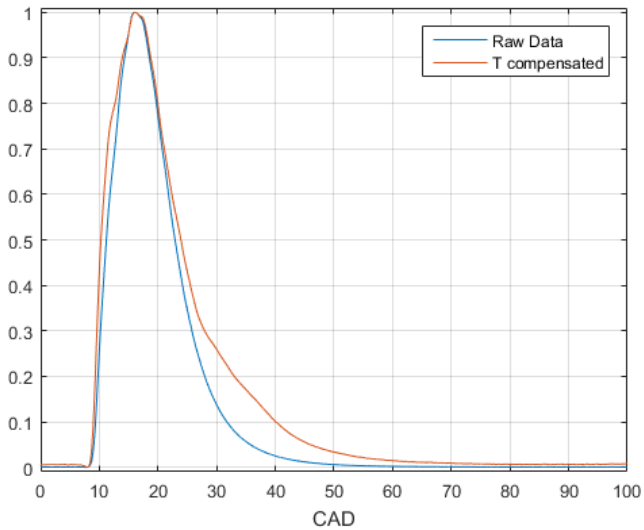

Figure 3.3 The blue curve is the natural luminosity of the soot shown here for an optical engine as a function of time (CAD), the red curve being based on the same data but with the temperature compensated for.

3.3 Laser induced fluorescence

Laser induced fluorescence (LIF) has been widely used for decades for combustion diagnostics [29]. To illustrate the principle involved in LIF for a species with only two energy levels, one can note that if there is an exciting source that provides the same degree of energy between two levels as the specie's absorbing energy does, a population conversion occurs, such that the species absorbs the energy and goes into a higher energy state, spontaneous emission from the excited species then being released. This emission is so-called laser induced fluorescence.

OH is one of the most commonly probed species used in combustion diagnostics [17]. One reason for this is that OH is a marker of the reaction region, the results obtained for OH being highly relevant for modelers and researchers in this area. Another

reason is that the absorption lines of OH shown a low degree of interference by other species. The signal strength of OH-LIF is also sufficiently high in an ambient flame.

The most commonly used type of OH-LIF excitation is that occurring on the basis of $A^2\Sigma^+$-$X^2\Pi$ (0,1) transition. The wavelength of the laser absorption line is at around 283 nm. Another excitation line is that through the $A^2\Sigma^+$-$X^2\Pi$ (0,0) band at 308 nm. However the OH-LIF also emits at 308 nm. The scattering of the laser light when a 308 nm laser is used for OH excitation should be carefully shielded against. Since in using a 283 nm laser for excitation the excitation wavelength is different from the emission, the scattering of the laser light can be suppressed by employing an appropriate filter, such as a 290 nm long pass filter or UG11.

Formaldehyde (CH_2O) is an intermediate species present in chain combustion reactions. It is used as a marker of the preheat zone [30, 31]. The absorption spectrum of CH_2O is broadband absorption from 250 to 360 nm, its fluorescence emission being present from 350 to 550 nm [32].

In studying the fuel consumption process, fuel tracer LIF can be used for detection of the fuel distribution. Acetone is one of the most commonly used fuel tracers. The absorption and emission of acetone is also broadband.

Table 3.1 summarizes different experimental arrangements used for various species employed in the thesis work.

Table 3.1 The experimental arrangements used for different LIF species in the thesis work.

Species	Excitation wavelength	Detection wavelength	Filters
OH	284 nm	308 nm	290 LP/UG11
CH_2O	355 nm	385-550/>400 nm	GG385/400 LP
Acetone	284 nm	>400 nm	400LP

3.4 Laser-induced incandescence

LII occurs when particles, which are usually soot, absorb incident laser radiation, and are heated to temperatures far above the ambient flame temperature, which greatly increases the amounts of blackbody radiation that occurs as compared with only ambient particles being present [29]. Since the absorption source is usually soot, both the absorption and the emission linewidths are broadband. The fundamental level,

1064 nm, or the second harmonic, 532 nm of an Nd:YAG laser are often used here [17]. In the thesis work, the fundamental wavelength was employed for reducing as much as possible absorption from polycyclic aromatic hydrocarbons (PAHs) or other species, except for soot.

The LII emissions exhibit a very rapid rise. An increase in the power of the laser pulse leads to an increase in the soot temperature. According to the Planck radiation law for blackbodies of the same soot volume, the higher the temperature is, the higher the radiation intensity becomes. This does not mean, however, that the laser pulse power being higher is better. Since an increasing proportion of the laser power becomes absorbed gradually by the soot particles, the laser pulse power finally becomes attached almost entirely to the small carbons molecules that are present.

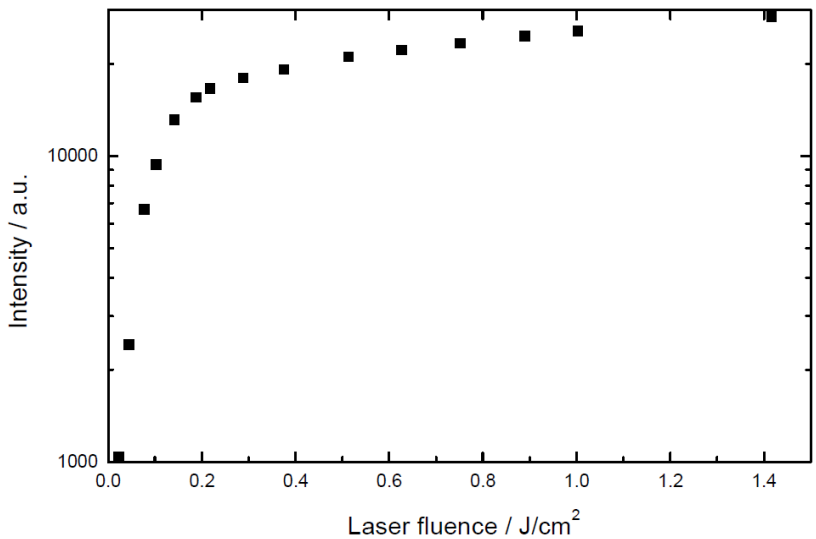

Figure 3.4 The laser power sweep for LII.

A plot of the laser power sweep is presented in Figure 3.4. As can be seen there the intensity of the LII signal that is emitted reaches a 'plateau' when the laser power becomes higher than 0.2 J/cm^2. The exact level of the 'plateau' of the LII signal has been shown to be proportional to the volume fraction of the soot which is present [33].

In summary, LII can be employed for 2D measurement of the soot volume fraction through use of a laser of sufficient power and of an ICCD camera for detection purposes. In the thesis work, the LII results were used only for detection of the soot distribution.

3.5 Laser extinction measurements

LEM is a line-of-sight measurement. A schematic diagram of LEM is shown in Figure 3.5. In sending a laser through a medium of interest, the laser intensity both before (I_0) and after (I) was measured. The degree of transmittance of the soot cloud can be related to its optical density through use of Beer-Lambert's law, the KL factor, used as a metric to describe soot measurements, being calculated by use of Equation (3.2)

$$e^{-KL} = \frac{I}{I_o} \tag{3.2}$$

Here, K represents the mean extinction coefficient along the beam path and L represents the length of the absorbing medium. K consists of two parts: scattering and absorption. If the particle sizes are much smaller than the laser wavelength the scattering is assumed to be negligible. It has been generally assumed that extinction brought about by the presence of soot is dominated by absorption rather than by scattering[15]. In the case of an optical engine, L varies over time and cannot be measured easily. KL is related to the optical density of soot [15] and is used in the present work as a metric for describing measurements of soot.

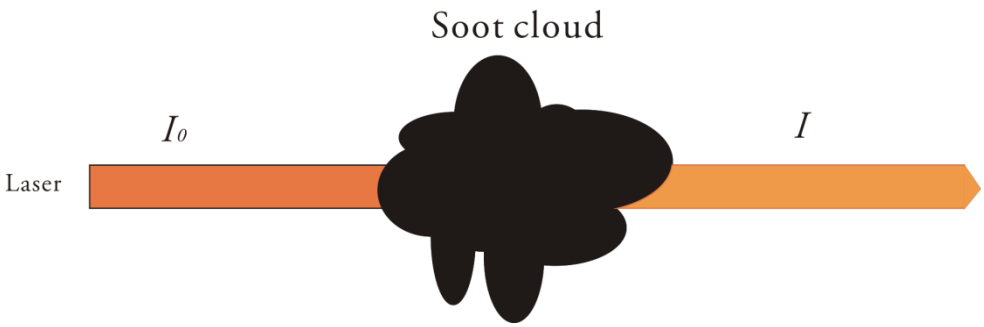

Figure 3.5 A schematic of LEM.

In contrast to natural luminosity data, LEM data does not depend upon the temperature of the soot involved. The fact is that the soot which is present absorbs laser energy, regardless of the temperature of the soot. This provides the possibility of probing of low temperature soot when the low soot natural luminosity is too low to be detected. Since the LEM principle appears quite straightforward, only a relatively simple setup is usually required. Time-resolved LEM data can be collected by use of either a continuous laser or a high-frequency pulsed laser.

As mentioned in earlier sections, a laser of short wavelength can be absorbed by molecules other than those contained in soot particles. A 685 nm laser was chosen for LEM in the thesis so as to minimize the absorption of the laser by other species.

Further information regarding the alignment of the laser can be found in Papers V and VI.

4 Experimental work - OH optical diagnostics

The study of OH radicals has taken place since the 1960s [25, 34]. People started to study OH radicals in connection with their chemiluminescence [25], OH-LIF then being introduced to flame measurement [35]. In the thesis work, both OH* chemiluminescence and OH-LIF have been employed.

In this chapter, a short summary of the OH optical diagnostics results of Papers I to V will be provided at the beginning of each section. In addition, further results from measurements similar to those made in already published works are presented and discussed. The challenges encountered and various suggestions regarding approaches that could be taken, thought of during the experimental work, will be discussed.

4.1 OH* chemiluminescence

As indicated in section 3.1, OH* chemiluminescence can be used to measure flame LOL [26]. However, collection of the OH* chemiluminescence signal suffers from high background levels of soot radiation. In optical engine applications, this high background level of soot radiation, in which soot clouds are recirculated toward the center of the combustion chamber after impinging upon the wall of the piston bowl, is especially obvious. Accordingly, the attempt was made in the studies reported in Papers I and II to reduce the effects that the background of natural soot incandescence luminosity had on the images obtained. It helps to reduce part of the soot luminosity from the OH*chemiluminescence images. An improved non-linear regression model to predict the flame LOL was also developed statistically on the basis of the LOL data calculated from the subtracted OH* chemiluminescence images in Paper II.

As can be seen in Figure 4.1 combustion does not start immediately after the fuel has been injected. The flame LOL is defined as the distance between the injector and the start of the flame.

The idea behind the online/offline method employed here was to take two images simultaneously with two different filters. One filter had a transmission range appropriate for the OH* chemiluminescence line, the other filter having a transmission range slightly outside that of the OH* chemiluminescence line. A band-pass filter centered at 310 nm (10 nm FWHM) served as the on-line filter both in Papers I and II, whereas a band-pass filter centered at 330 nm and one centered at 365 nm (10 nm FWHM) served as the offline filter in Paper II and Paper I, respectively. Both the OH* chemiluminescence and the background from the spectrum in Figure 3.1 in the online image are recorded, whereas the off-line image was only to contain the background. The background could be removed from the on-line images by subtracting the off-line images from them.

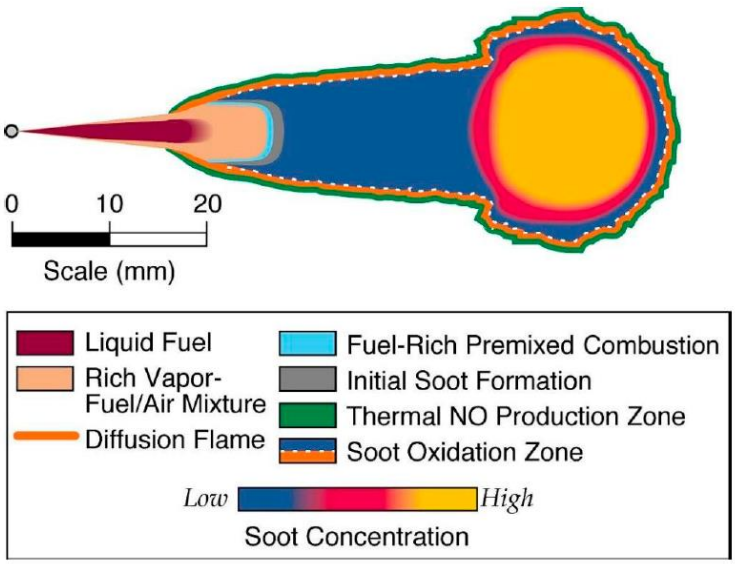

Figure 4.1 A conceptual model of the soot concentration as replotted from the finding of John Dec [36].

Before applying this method to the optical engine, testing of it on a candle flame was carried out, an example of this being shown in Figure 4.2.

A candle flame is a diffusion flame. The orange color of it stems mostly from hot soot radiation. In Figure 4.2, the online image is shown to the left, the offline image in the middle, and the binary image after background subtraction to the right. Since the candle flame is present under room conditions, the OH* chemiluminescence is weaker there than that found in a condensed environment such as in an engine.

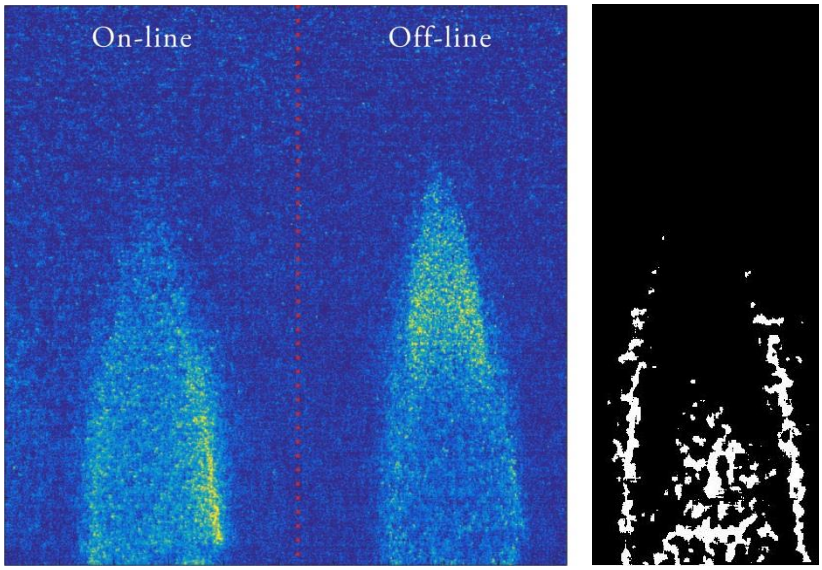

Figure 4.2 An example of online offline subtraction from a candle flame

Since different filters have different transmission curve, the ICCD sensors also differ in their sensitivity to different wavelengths, the radiation intensity of the soot also varying with its wavelength. In the testing carried out, the images were transformed to binary images before the subtractions were made, since OH is formed in the reaction zone where high temperature heat release occurs [37]. As shown in Figure 4.1, the OH can be detected in the soot oxidation zone. In Figure 4.2 the two OH 'lines' in the subtracted image can be observed as would be expected, whereas in the raw images no such shape can be clearly observed. This shows that, through use of this online/offline method in a stable diffusion flame, the location of the OH could be successfully highlighted after the subtraction.

Figure 4.3 presents sketches of a stereoscope in which two sub-images can be projected on a single sensor chip in a single exposure, each sub-image having only half the resolution of the original image, however.

As can be seen in Figure 4.3b, if the projection area of the target is larger than half that of the chip, the signal goes along path B and crosses with the signal that goes along path A. Depending on how the camera objective and the target are placed, a 'ghost' image from path B can sometimes be found on image A, and vice versa. When the stereoscope is mounted close to the target, the 'ghost' image effect tends to be very slight. However, in the optical engine measurements, the camera and the stereoscope were mounted close to the engine and collected data through the piston extension. The distance from the target to the stereoscope was usually more than 70 cm. To

keep this 'ghost' image effect at a minimum, it is best to reduce both the area of interest within the field of view and to minimize the background as much as possible. As can be seen in Figure 4.3c, a shield was added to reduce the cross-talk between the two optical pathways. In addition, with regard to the optical engine study that was to be carried out in the thesis work, and the fact that since the optical piston was round whereas the ICCD chip was square, and that more than one spray was to be included in the image, the two sub-images were moved away from each other so that they became located close to two opposite corners of the image field of the sensor chip.

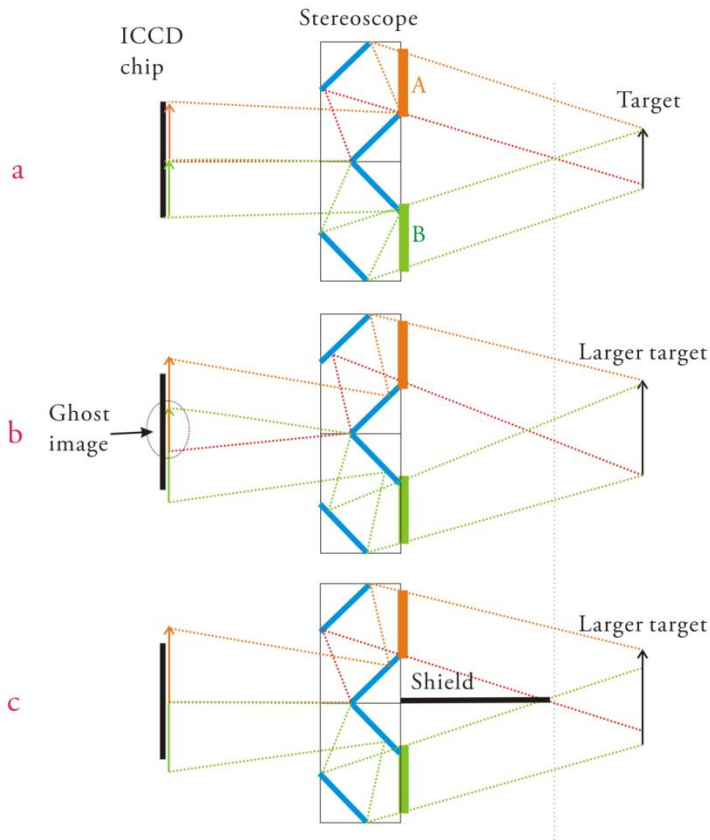

Figure 4.3 Sketches of a stereoscope and of a ghost image produced by it.

This online/offline method was applied to the optical engine for LOL detection in both Papers I and II. In the measurements carried out, a high speed intensifier was used for OH chemiluminescence detection. An example of such stereoscopic imaging is shown in Figure 4.4. The injector was a four-hole injector, three separate sprays being captured in the image. The online image is to the left, the offline image is in the middle, and the subtracted image to the right. The white dot on the image indicates

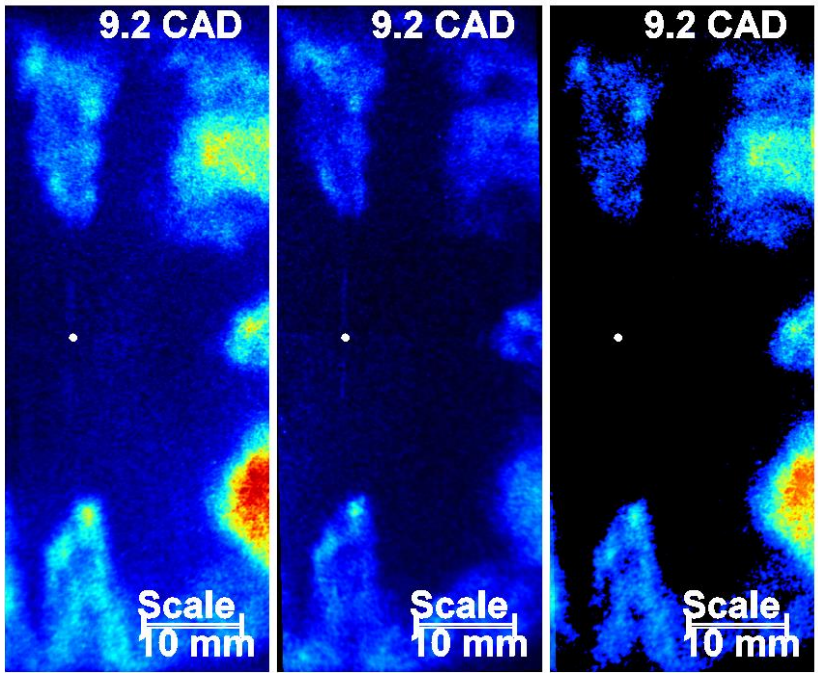

Figure 4.4 Stereo images with the online image being shown at the left, the off-line image in the middle, and the subtracted image at the right.

where the injector is located. Two flame structures can be recognized, in the 12 and the 6 o'clock location, respectively. Only part of the flame structure at the 3 o'clock location is captured in the image. For most of the cases the start of flame at the 3 o'clock position can be captured in the image, this being sufficient to calculate the flame LOL. The LOL result obtained by use of this method was used to analyze the effects of the engine parameters on the flame LOL.

4.2 Comparison of OH-LIF and OH* chemiluminescence

In this section, the fuel fluorescence problem is taken up and the matter of the flame axis-asymmetry is discussed further. At the end, the images obtained with use of different offline filters are presented, the observations made being discussed.

OH* chemiluminescence is not the only approach that can be used for identifying flame LOL. OH-LIF is an alternative approach that can be used in flame liftoff

studies [38, 39]. In Paper I, a comparison of OH-LIF and OH* chemiluminescence for the measurement of LOL was performed. By applying simultaneous OH-LIF and OH* chemiluminescence to an optical engine, the effects of cycle-to-cycle variations could be successfully minimized. The LOL as determined by OH-LIF was found to be longer than that determined statistically on the basis of OH* chemiluminescence. The LOL 'bias' as calculated by use of these two respective methods can be explained on the basis of the differences between the two methods in the flame axis-asymmetry and the probing volumes involved.

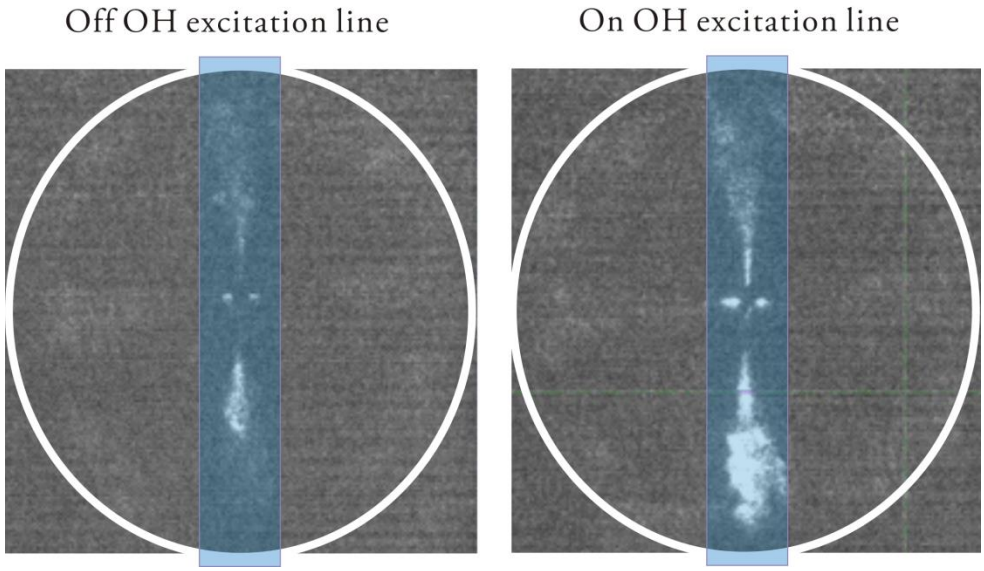

Figure 4.5 Images of the fuel fluorescence obtained with the exciting laser being on or being off the OH line.

In studying the diesel combustion process, there are many challenges that can be encountered in connection with LIF-based measurements, such as regards matters of spray formation, fuel evaporation characteristics, in-cylinder fluid flow and combustion chemistry, the latter including matters of pollutant formation, especially when the engine is running on commercial-grade diesel fuel. The dense fuel spray can not only effectively trap laser and signal light but it can also redistribute laser and signal light through multiple scattering. Downstream in the spray, soot can be present in high concentrations, its also trapping laser and signal light and providing scattering [40]. Satbir and coworkers [41] have reported that a high degree of soot formation and diesel fuel fluorescence can make it difficult to detect OH-PLIF from the upstream part of the burning jet.

During preparation for the experiments that were carried out here, it was found that for reasons in addition to those referred to above, the excitation laser for OH, which was at 284 nm, could excite not only OH but also the impurities in the fuel. At the beginning of the project, the fuel employed was normal commercial n-heptane of 95% purity. As can be seen in Figure 4.5, regardless of whether the wavelength of the laser was on the OH excitation line or not, there was always a fluorescence signal from the fuel and the signal could not be removed by the OH filter. It was not scattered light from the fuel either, since later, when the fuel and the fuel pump system were improved, this signal from the fuel disappeared. Different grades (degrees of purity) of n-heptane were tested, its being found that the highest grade (spectral grade) n-heptane (with a purity of over 99.9%) fluoresced the least.

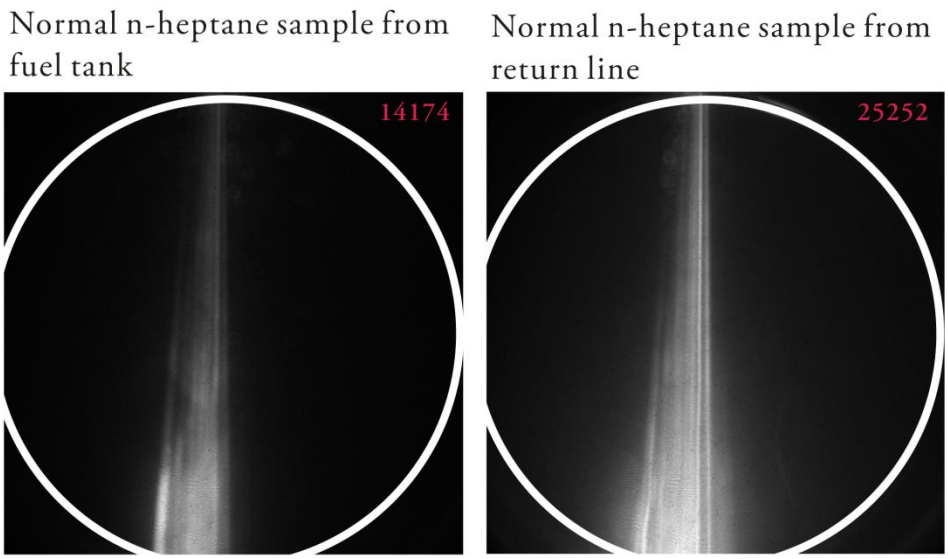

Figure 4.6 Images of the fuel fluorescence.

As mentioned earlier, the optical engine was a modified product-type engine. The original fuel pump system was the same as that in the product engine. It was found that this fuel pump system resulted in undesired fluorescing sources being added to the fuel. Figure 4.6 shows test images from the fuel before and after it has passed the fuel pump. The image at the left shows the fluorescence stemming from n-heptane in the fuel tank, whereas the image at the right shows fluorescence by the fuel sample coming out from the high-pressure fuel pump through the return line. The images were taken through the optical engine, the white circle indicating where the bowl wall of the optical piston is located. The fuel was poured directly into the piston bowl, and the laser was transmitted through the liquid fuel from the lower to the upper part of the image. The number in the upper right corner indicates the maximum pixel

intensity for each of the two images. Both images were taken with use of the same laser power, filters and camera settings. As can be seen, it is brighter in the middle part of the right image than in the left image and the maximum signal intensity of the right image is almost twice that in the left image. Thus the fuel was 'contaminated' by the original fuel pump system, this contaminating fluoresce being more than that in the fuel itself. In order to continue with the LIF measurements, the fuel and the fuel pump system would need to be improved.

During the experiments, at each time the fuel was changed, the entire fuel pump system was flushed at least three times by a sample of the fuel to be involved. This process usually consumed about 15 L of fuel, regardless of when it took places. In view of the high price of spectral grade n-heptane, in the end analysis grade n-heptane (>99.0%, from Merck) was found to have the best balance between economy and the fluorescence-free signal that was to be used in the thesis work.

Also, to keep the waste of fuel for flushing and problems concerning with undesired fluorescence caused by contaminants at a minimum, a clean chemically resistant fuel supply system making use of appropriate pump and filter material, hoses, gaskets, and sealant materials and small in volume, was designed for use during the thesis work.

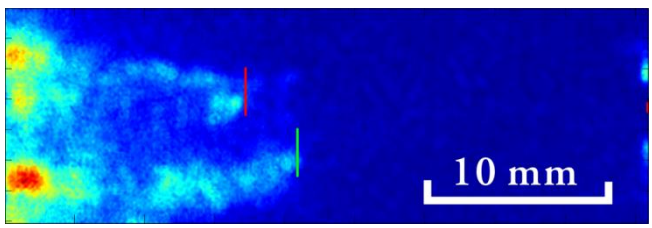

Figure 4.7 An illustration of the procedure employed for the calculation of LOL

Through the efforts made to change to as clean a fuel pump system and as pure fuel as possible, the fuel fluorescence could be successfully removed from the OH-LIF image, as can be seen in Figure 4.7. In that figure, the red dot on the right end in the image indicates where the injector was located. Due to the limits to the size of the laser sheet only one of the four sprays was probed. Two separate OH 'belts' located on each side of the spray axis can be seen in the image here which makes it different in this respect from the chemiluminescence images. From Dec's conceptual soot model [36], it is known that the OH radicals are located mainly in the high-temperature reaction zone close to the outer surface of the flame. The same phenomenon was observed in [42]. The two regions that can be seen in Figure 4.7 are the result of the laser sheets only illuminating a relatively thin cross-section of this outer shell.

The 'bias' is calculated in Equation (4.1).

$$Bias = \frac{LOL_{LIF} - LOL_{Chemi}}{(LOL_{LIF} + LOL_{Chemi})/2} \times 100 \quad (4.1)$$

It is known that the down-swirl LOL is usually shorter than the up-swirl [27]. In order to see whether the 'bias' is linked to the up-to-down difference in swirl LOL, a parameter to scale the asymmetry of the swirl was needed. The LOL 'difference' found here between up- and the down-swirl is defined in Equation (4.2)

$$Difference = \frac{LOL_{Down-swirl} - LOL_{Up-swirl}}{(LOL_{Up-swirl} + LOL_{Down-swirl})/2} \times 100 \quad (4.2)$$

Obviously the greater the 'difference' is, the more asymmetric the flame is in the swirl plane. In the work carried out, all of the 'difference' involved is calculated in this way and is displayed as a percentage.

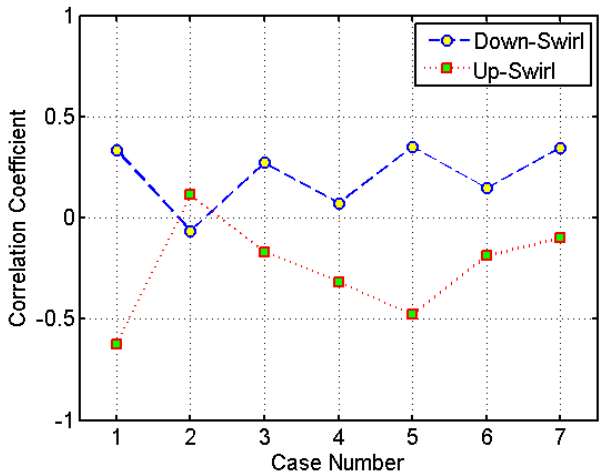

Figure 4.8 Each point that is shown represents the value of the correlation coefficient between the 'bias' and the 'difference' involved.

Two 'differences' can be calculated for each cycle from LIF and from the chemiluminescence images, respectively. In this section, the chemiluminescence 'difference' is employed, since it is more vertical plane symmetric than the LIF 'difference' is due to the larger probing volume involved. Correlation coefficients were calculated between the 'bias' and the 'difference' in chemiluminescence for the up- and down-swirl, respectively. As taken up in Paper I, 7 different engine conditions were distinguished, numbered as cases 1-7. A plot of the correlation coefficients for all 7 cases is shown in Figure 4.8.

As can be seen in Figure 4.8, there is very weak correlation between the 'bias' and the 'difference'. This can also be understood as that there being a very weak correlation between the 'bias' and the degree of asymmetry in the swirl plane. In the work as

carried out, effects of the asymmetry in the vertical plane cannot be measured, since no side-view data on this engine is available. Figure 4.9 shows a sketch of the quartz piston cross-section. It can be seen that this is due to the probing volume of the laser being smaller than that of the flame, the LOL as measured by the two techniques thus always being biased. The 3D 'bias' here is defined in Equation (4.3).

In terms of Equation (4.3), the 3D 'bias' is proportional to sin(a). If the flame were not symmetrical in the vertical plane, the angle 'a' would not be equal to the umbrella angle of the spray, so that the asymmetry in the vertical plane would affect the 'bias' that was present.

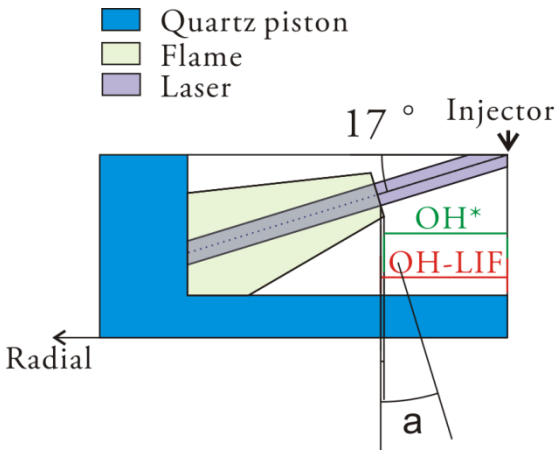

Figure 4.9 A side view of the signal-collection geometry.

$$Bias_{3D} = \frac{Flame\ Diameter - Laser\ thickness}{2} \times |\sin a| \qquad (4.3)$$

A boxplot of both the down- and the up-swirl 'bias' from one of the 7 cases is plotted in Figure 4.10. The plot at the left shows the LOL 'bias' present in the down-swirl region and the plot at the right shows the corresponding 'bias' for the up-swirl region. The mean LOL 'bias' for the down-swirl is less than that for the up-swirl and the LOL 'bias' varies within a greater range for the up-swirl than that for the down-swirl.

A potential explanation for this could be the 3D effect. From the 3D 'bias' graph in Figure 4.9, one can see that the flame volume covered by the laser sheet is the same in the downstream region of the fuel spray as in the upstream region of it, but that the flame expands more downstream than upstream. Accordingly, the laser covers a lesser portion of the total flame volume downstream than it does upstream. In reality, however, the flame has a 3D structure that is not perfectly symmetric in its axis. Since as mentioned earlier the LOL is usually longer in the up-swirl, which refers to what is further downstream, there is a greater possibility for the laser sheet to miss the part of the flame front in the up-swirl lift-off region that is used for calculating the LOL.

Whereas, the LOL measured by chemiluminescence always shows the shortest distance, the LOL 'bias' between the two techniques has a larger variation in the up-swirl region.

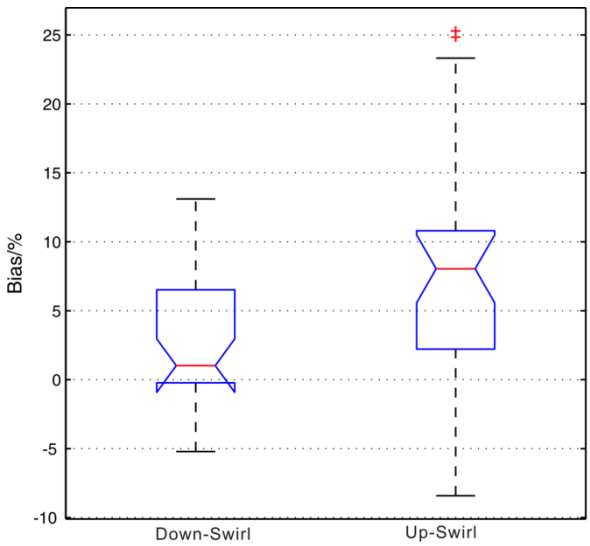

Figure 4.10 A boxplot of two data samples from the down- and the up-swirl LOL bias, respectively.

Another explanation for the mean LOL 'bias' for the down-swirl being less than for the up-swirl could be the non-perpendicular collection angle in this engine configuration. The cameras were recording from a bottom view through the transparent quartz piston, yet the sprays have a certain umbrella angle. In Equation (4.3), when the angle 'a' differs from 'zero', the 'bias' is ideally related to the difference between the diameter of the flame and the thickness of the laser. When the angle 'a' is fixed, the 3D 'bias' is greater in the downstream than in the upstream direction.

Figure 4.11 shows the mounting of the cameras and the stereoscope. The two ICCD cameras were mounted perpendicular to one another in the same plane. The online/offline method was employed first in Paper II. The offline filter used in Paper II had a transmission range centered at 330 nm. In looking at the flame spectrum in Figure 3.1, the background luminosity level can be seen to increase with wavelength. It is better to have the transmission range of the offline filter as close to 310 nm as possible. In Paper I, however, a 365 nm band pass filter was used instead. This is because of the OH-LIF signal being within the same wavelength range as the OH* chemiluminescence, and in that experiment a dichroic mirror being used to separate the OH-LIF signal from the offline image. Since this dichroic mirror only transmits

signals having a wavelength greater than 350 nm, a 365 nm filter was used in Paper I instead. A comparison of the images transmitted by the 330nm filter with the images transmitted by the 365 nm filter was made. There was to be no significant difference found between images recorded through these two filters.

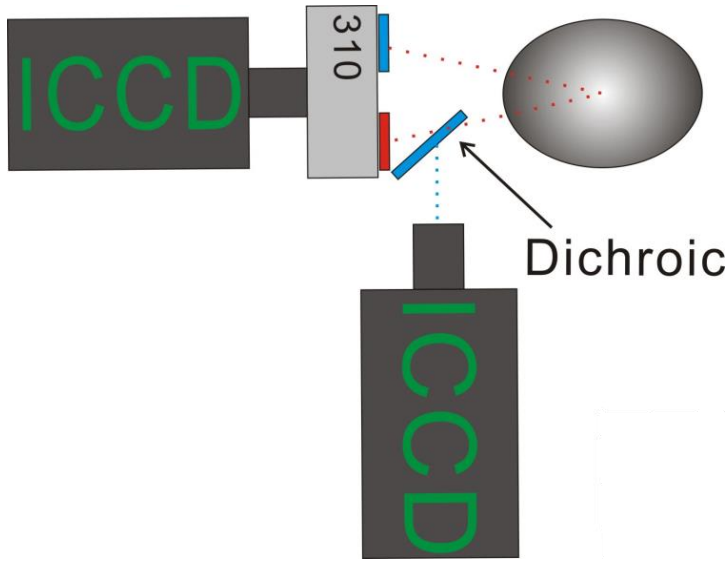

Figure 4.11 The setup of the cameras and the stereoscope

In an earlier study by Siebers [43], a comparison of the OH* chemiluminescence with the soot incandescence in a constant volume vessel was presented. In that work, the incandescence signal was found to be emitted further downstream in the flame than the OH* chemiluminescence signal was. Since this is not what was observed for the offline images in Papers I and II, a further test was performed, a 550 nm long pass filter being used as the offline filter instead.

The images obtained with use of the different off-line filters are shown in Figure 4.12. Image A is the raw image obtained from the stereoscope camera with use of 310 and 365 nm filters. The number on the image indicates which filter was employed. Due to the filters differing in their transmission range, the two sub-images are not of equal brightness, yet despite the brightness differing, the flame structure in the upstream part can be recognized for image A in both sub-images. Image B is cropped from image A. Image C, involving use of 550+ offline filter, was taken under the same engine conditions as the others. In comparing image B with image C in Figure 4.12, one can note that part of the flame, which is indicated by a rectangular, cannot be clearly recognized in image C in comparing it with image B. What is shown in image C is similar to what Siebers presented in [43]. If image B and image C show a similar soot distribution, why is there such a difference?

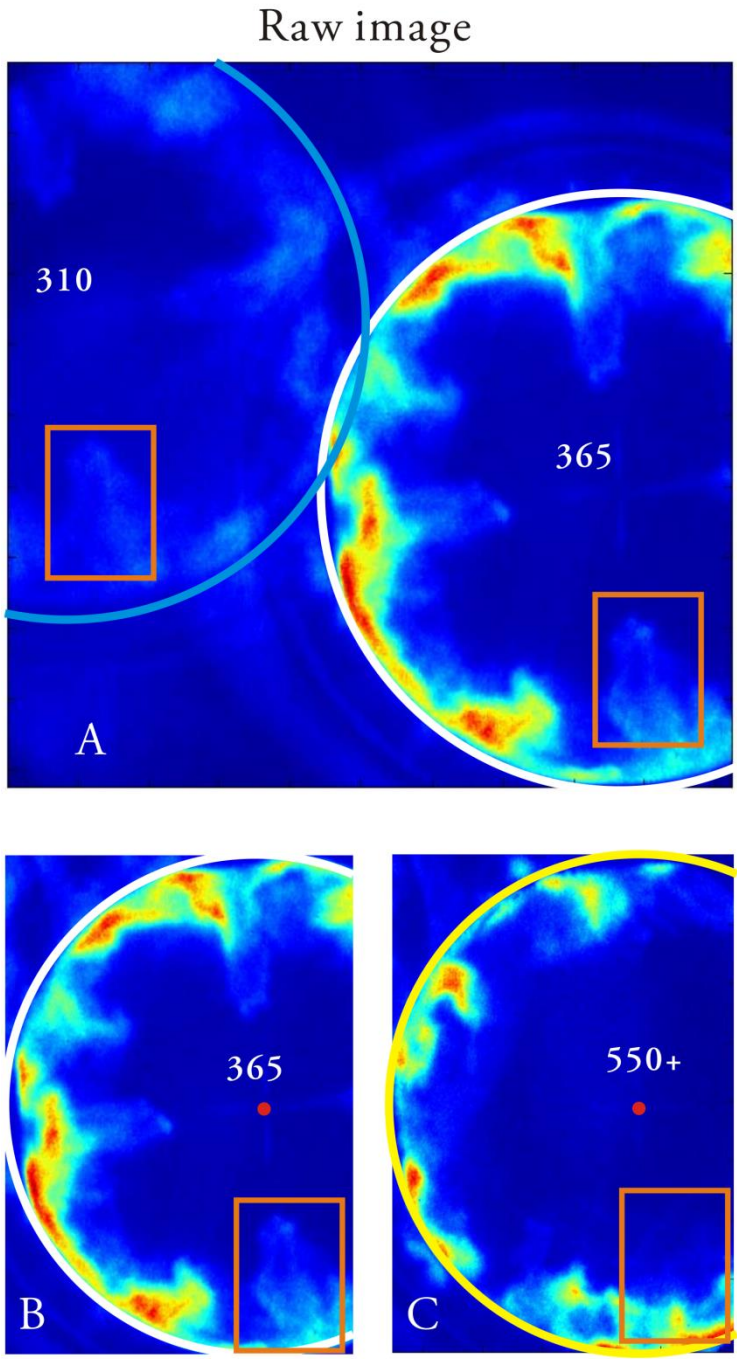

Figure 4.12 Images taken with use of different filters.

From Dec's soot model it is known that the soot concentration tends to be lower in the upstream than in the downstream direction. The flame temperature is also lower in the upstream direction [44]. Assuming the incandescence signal to be produced entirely by soot radiation, the radiation intensity should, according to Planck's law, depend upon the wavelength and the temperature.

The author suspected that for image B both the upstream and the downstream soot radiation at 365 nm would be relatively low, so that the difference between these two regions would not be as great as in the case of image C with use of a 550+ filter. However, since for image C the radiation intensity was found to be relatively high, especially at higher temperatures, so as to not to saturate the camera a lower gain value and extra ND filters were employed. The differences between the high-temperature and high-soot-concentration parts of the setup (downstream) and lower-temperature and lower soot-concentration part (upstream) are considerable. Because of the limited dynamic range of the detector, when the downstream part is shown, the upstream part is too low to be seen or even to be detected through the use of extra ND filters. Thus, the face that image C only provides information concerning the high-temperature and high-soot-concentration parts of the setup does not mean that there is no soot in the remaining parts of the flame.

This appears to the author to be a plausible account of the conclusions one can draw here. Although there could be other interpretations of the facts at hand, these will not be discussed here further.

4.3 High-speed simultaneous PLIF imaging of two species

The high speed imaging method for diagnosing turbulent flames was introduced in the late 1990s [4]. Different types of laser system are used for high-speed laser diagnostics. In the thesis work, the multi-YAG and the framing camera are employed in connection with the turbulent flame experiments. In section 4.3.1 a novel way of probing two different species simultaneously is presented. Paper IV demonstrates the use of this for the simultaneous probing of OH and of formaldehyde-PLIF at a repetition rate of 50 kHz. Use of this time-resolved dual-species data enabled turbulent flame extinction and re-ignition to be captured. The results of high speed OH and acetone-PLIF by use of a similar setup is presented in section 4.3.2.

4.3.1 High-speed simultaneous OH and formaldehyde-PLIF

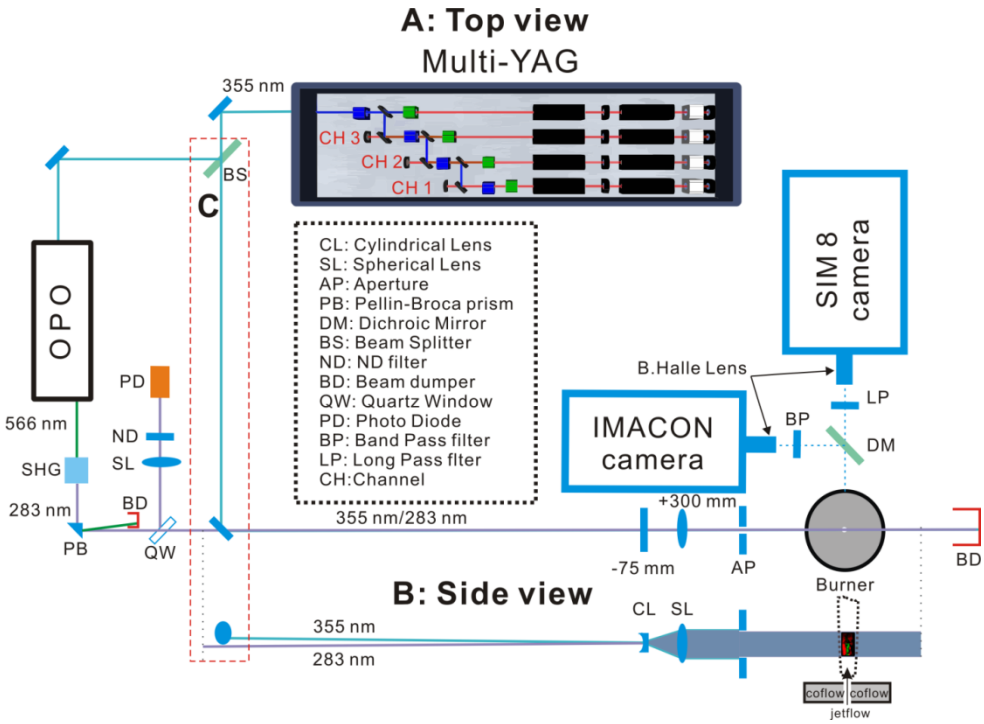

Figure 4.13 A sketch of the experimental setup used for high speed dual-species-PLIF.

Figure 4.13 shows a sketch of the experimental setup used for high-speed dual-species PLIF. In order to balance the laser power of all the pulses in a single burst, an online laser power monitoring line was used here. A quartz plate was placed after a Pellin-Broca prism, 1-2% of the laser beam being reflected by this quartz plate and focused on the photodiode. To avoid signal saturation, ND filters were mounted in front of the photodiode, as shown in Figure 4.13. The laser beam was never fully shielded, there always being scattered laser light or laser induced signal from the room. Normally, such signals can be detected by a photodiode so as to check the laser timing. However, the intensity of this scattered signal is not necessarily proportional to the laser power involved.

For a double-pulse mode of the multi-YAG laser, the Q-switch delay between the first and the second pulse was used to change the temporal pulse separation and the relative power of two pulses in a given channel. The λ/2 plate in each laser channel was used to tune the laser power in the different channels within a small range. Before balancing the laser power of all the pulses contained in a single burst, the laser power was first optimized to the maximum in each channel each time the laser was started. After that, through changing the Q-switch delay and the λ/2 plate the laser power is balanced from pulse to pulse in a single burst. During this process, the signal intensity

produced by the online monitoring photodiode was used as a reference. Usually this process took one to two hours each time. In Figure 4.13, it can be seen that in a multi-YAG laser all the laser pulses go through the third harmonic generation (THG) crystal in channel 4. Although the THG should not absorb very much of the 355 nm radiation, it was found that the THG in channel 4 became overheated after 2-3 hours of being run continuously. Unfortunately the THG crystals in this system were not water-cooled. As long as the THG was overheated, the power balance between the pulses, as well as the laser beam profile, could readily change. By tuning of the angle of THG in channel 4, the laser beam profile and power could be re-balanced. However, since there was no coolant for the THG crystal provided, its temperature would continue to increase. This would lead to the angle of it needing to be re-balanced again within a few minutes. It would be almost impossible to continue with the measurement taking very long under such conditions. It can be suggested that as long as the THG crystal is overheated, the laser should be stopped and started again when it is fully cooled down. Thus, the problem of the overheating of the THG crystal is unavoidable with use of the current laser arrangement. Each time the laser starts, there is only about a one-hour time window available for the recording of data.

It should be noted that the 4 channels should all be turned on at once during the balancing process here, since channel 1 and channel 2 share a single cooling pump, and the same is true of channels 3 and 4. If only channel 1 is in use, then in turning on channel 2 the power of the laser available from channel 1 would change.

The OPO was used in this setup for converting the laser wavelength to 566 nm. Since the wavelength of the output laser and the power that the OPO provides depend upon the angle of the input laser, all the laser pulses from the different channels need to thoroughly overlap. In the present work, the spatial overlap of the laser pulses was checked for a distance at least up to 20 m from the multi-YAG.

In OPO, a 355 HR dichroic mirror is placed between the two cavity mirrors, as shown in Figure 4.14. Thus part of the input laser is reflected by the cavity mirror and follows the same path as the input laser, but in the opposite direction. The back reflection power of the laser from OPO is about 20% that of the input laser. When the multi-YAG operates at full power, 20% of the laser power is sufficient to damage the optics or the laser cavity if the back reflection of the laser clips off the edge of them. For this reason, the back reflection of the laser needs to be tracked and properly dumped. A 355 HR dichroic mirror and a laser beam dump located between the THG and the second harmonic generation (SHG) crystal in channel 1 of the multi-YAG were added.

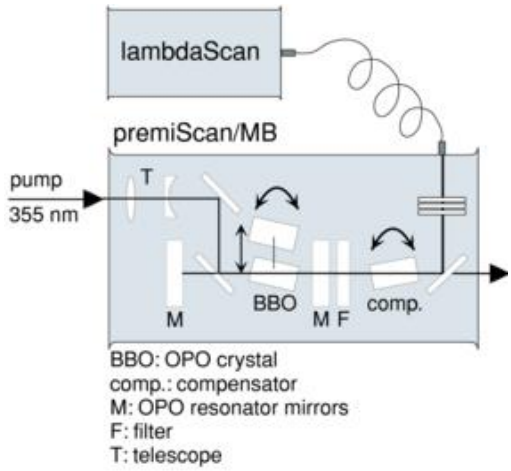

Figure 4.14 A sketch of OPO replotted from [19].

For the jet flame study, the flame was measured at different jet-flow speeds and equivalence ratios. The experimental conditions are shown in Table 4.1.

Table 4.1 Experimental conditions applying to the methane/air flame.

Equivalence ratio	$\emptyset = 1.0$		$\emptyset = 0.6$	
Jet-flow speed (m/s)	150	120	150	120
Co-flow speed (m/s)	0.16	0.16	0.16	0.16

A methane /air flame was used in this case. In order to only study the effects of the jet-flow speed and the equivalence ratio, the co-flow conditions were kept constant (hot gas being generated by the pilot flame of methane/air at 0.16 m/s, where Φ=1). The imaged area was 11 mm wide and 20 mm high, its extending from 25 mm to 65 mm above the burner in each of two separate sections. The higher (downstream) region was chosen here, since the local extinction and the flame closure effects could be captured more frequently in this region of the flame.

Figure 4.15 shows a time-resolved series of simultaneously captured CH_2O-PLIF and OH-PLIF images of a turbulent premixed flame at a 120 m/s jet-flow speed, where Φ= 0.6. The images extend in a time sequence from left to right, there being a temporal separation of 20 μs between consecutive frames. In a conventional 10 Hz laser diagnostic experiment, a single OH breaking could be found, such as is shown in Figure 4.15. However, a time-resolved sequence following this OH breaking could hardly be recovered on the basis of 10 Hz measurements. Thus, high-speed laser diagnostics were necessary to obtain a visualization of the turbulent flames. A local

flame extinction process could be followed clearly in these images, as indicated by the solid yellow arrow in Figure 4.15A.

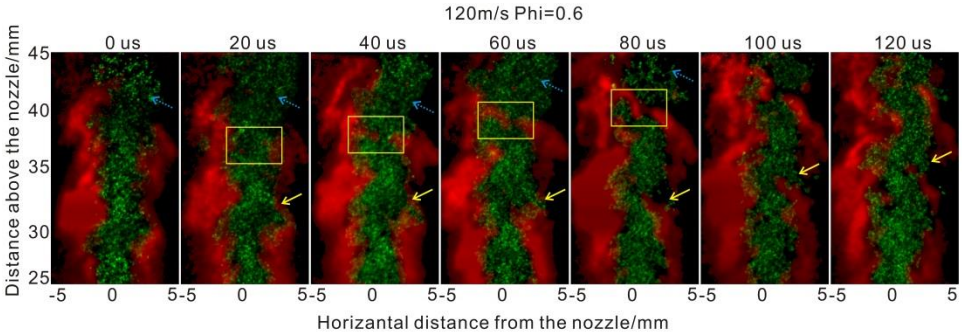

Figure 4.15 A time resolved simultaneous OH (red)/CH_2O (green)-PLIF images sequence.

By taking images simultaneously for OH and for CH_2O-LIF, it could be seen that the CH_2O was 'leaking' through the OH quenching hole. In the flame downstream, pointed at by the blue dashed arrow, a larger flame quenching area can be observed. A local extinction process can be followed in these images, as indicated by the solid arrow. Before the local extinction occurred, there was a section in the 0 μs image in which the OH layer was thinner than the surroundings. This thinner OH layer became even thinner in the 20 μs image that followed (see the second image), the OH layer then breaking in this thin region, the gap created increasing over time, as shown in the images that followed. When local extinction occurred, the CH_2O in the preheated zone was transported through the extinction point by turbulence eddies. During this process, the CH_2O could not rapidly be consumed in its entirety. For the burner, the jet flame got less support downstream from the co-flow flame travelling at a higher jet-flow speed [31]. The further downstream it came, the cooler the entrained gas became. A local relatively fuel lean and cooler area was formed around the extinction point. Under these conditions, the mixture could hardly be re-ignited [31] and consumed. In the flame downstream (shown as the upper part of the images) that the dashed arrow points to, a rather larger flame quenching hole can be observed, under which conditions it is obvious that CH_2O would not be fully burnt and that it would disappear into the surroundings.

Figure 4.16 presents images moving at 120 m/s and having an equivalence ratio of 1. A local flame quenching process can be followed in this image sequence, one highlighted by use of the dashed white square. Yet in this case CH_2O leakage from the OH break point was not found. In comparing Figure 4.15 with Figure 4.16, one can note that in the OH quenching area in Figure 4.16 the OH layer is thicker than that shown in Figure 4.15. As described in the previous section, when the OH layer is broken, this creates a gap in which the CH_2O can mix with the co-flow products. The

CH_2O has the tendency to flow through this 'gap', something one can also note in the image. However, CH_2O failed to fill up the OH quenching area there as it had in Figure 4.15. This is due to the OH layer being thicker there. Under such conditions, if CH_2O is to be transported through the 'gap' that exists to the cooler ambient air, it needs to penetrate a greater distance, so that there is sufficient time and heat for the CH_2O to be fully consumed.

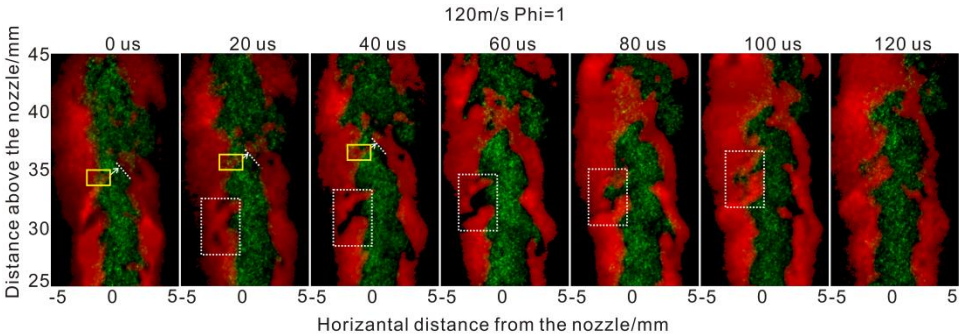

Figure 4.16 PLIF images of OH (red) and CH_2O (green). The images are shown in time sequence from left to right, there being a time separation of 20 μs between consecutive frames. The jet-flow speed is 120m/s and the equivalence ratio is equal to 1. Above the burner, the image is 11 mm wide and 20 mm high.

In Figure 4.15 and Figure 4.16, the yellow rectangular area indicates there to be a flame hole healing process taking place in the center of the flame. This flame hole healing phenomenon can also be found along the boundary of the flame such as is shown by the white dashed rectangular area in Figure 4.16. In the images there, a flame tip can be seen from the left part of the flame at the start. This flame tip propagates towards the other side and meets with the OH from high right side, a closed area formed by the OH surrounding it. After this the CH_2O in the part higher up either goes into the ambient air and mixes with it or is consumed in higher temperature regions outside the field of view.

When the flame tip is growing in size, there is some CH_2O still surviving in the 'fresh' OH area within the yellow rectangle, both in Figure 4.15 and in Figure 4.16. In a turbulent pre-mixed flame, the CH_2O is consumed within the reaction zone. Under highly turbulent flame conditions, however, rapid turbulent transport can make a trace amount of CH_2O available in the OH region. A similar effect can also be seen in the Figure 4.17.

Figure 4.17 shows the upper part of the flame, 45-65 mm above the burner nozzle. The speed of the jet-flow is 120m/s, the equivalence ratio being equal to 1 in the first row and 0.6 in the second row, respectively. In the upper part of the flame, unburned pockets can be found. These flame holes are formed in the lower part of the flames

through the inner flame healing. Some of the CH_2O in the flame holes is burned (pointed at by the solid arrow) and some leaks out through the flame quenching point (pointed at by the dashed arrow). Three different examples of a flame hole are shown in the images. Figure 4.18 was generated by calculating the pixel number of flame holes and CH_2O islands in a particular area.

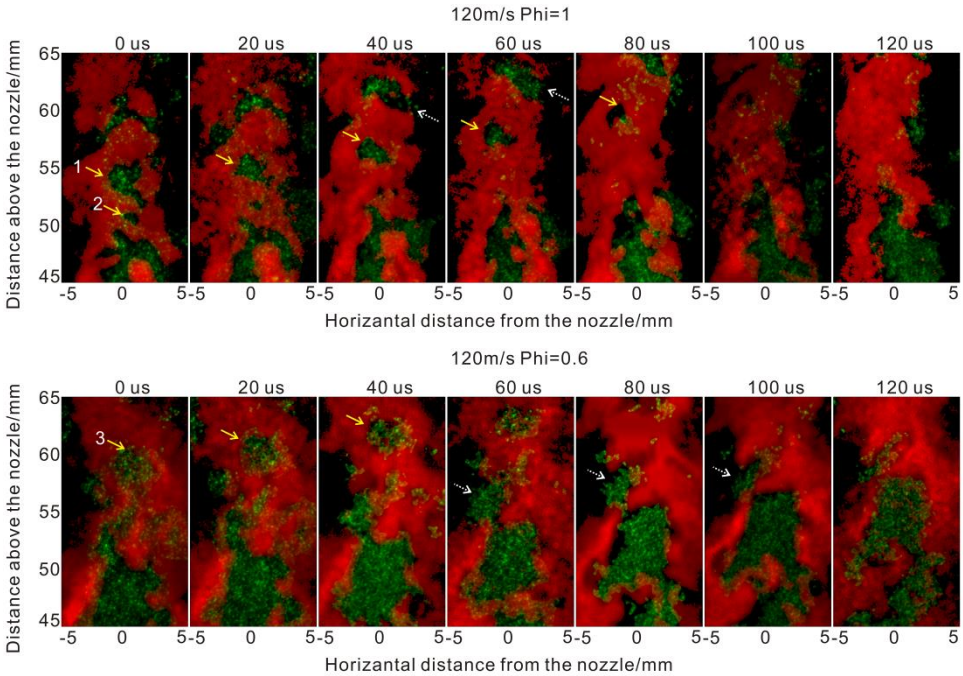

Figure 4.17 PLIF images of OH (red) and of CH_2O (green). The images are in a time sequence from left to right, there being a time separation of 20 μs between consecutive frames. The speed of the jet flow is 120m/s, the equivalence ratios being equal to 1 (in the upper images) and to 0.6 (in the lower images), respectively. The image is 11 mm wide and 20 mm high.

In Figure 4.18, concerning the same flame hole case as dealt with in Figure 4.17, the CH_2O area is always larger than the OH hole area, which also demonstrates that there is CH_2O left in the OH region. Here the CH_2O curve decreases faster than the OH curve did in the beginning. After awhile the two curves become nearly parallel until they both drop to zero. This corresponds to the process of the consumption of CH_2O pockets by OH.

Figure 4.19 shows images obtained under higher jet-flow-speed conditions, those of 150 m/s and an equivalence ratio of 1. Local flame quenching and CH_2O leakage can readily be seen in the downstream region of the flame (the solid arrow points at it).

Due to the limited size of the sample of images that have been collected under these flame conditions, flame-hole healing is rarely found in the lower region (25-45 mm height above burner). Further measurements are needed in order to correlate the flame healing with the presence of turbulent flows.

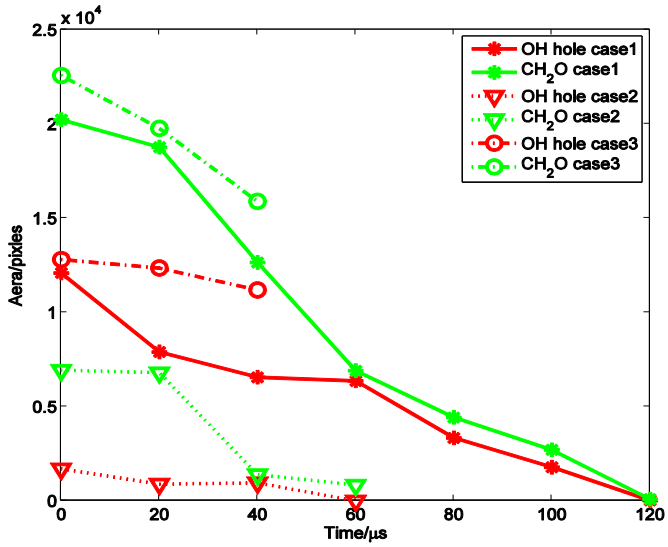

Figure 4.18 An OH hole and a CH_2O pocket area shown as a function of time.

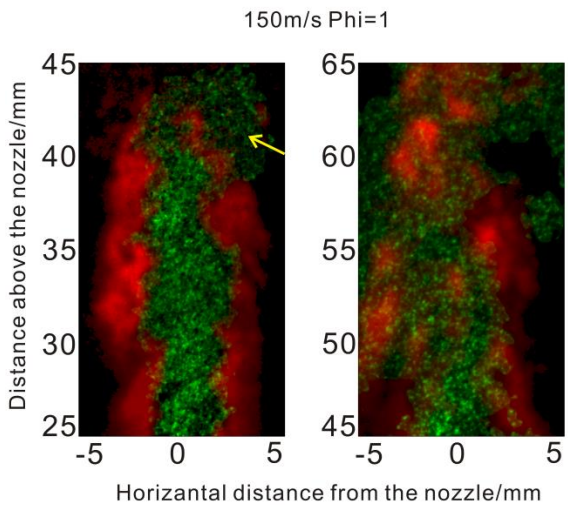

Figure 4.19 A PLIF image of OH (red) and of CH_2O (green). At the left an image obtained from region 25 to 45 mm above the burner is shown and at the right an image is from regions 45 to 65 mm above the burner.

The upper part of the flame of high jet-flow speed can be seen in Figure 4.19. Due to the high jet-flow velocity, the OH is broken up into many small pockets, yet one can still identify the OH structure. At the same time, the CH_2O-PLIF signal is present almost everywhere in the image. One reason for this is the fact that the flame that is present in the upper part of the region of high jet-flow-speed conditions has a higher turbulent level than that in the lower part does, so that the mixing rate induced by the turbulence can be higher than the chemical reaction rate. Another reason for it that is likely is that in the upper part, when the flame tends to break into small pockets, more ambient air entrainment is involved, leading to a lower temperature, whereas at temperatures < 1000K CH_2O typically lacks a consumption mechanism.

The recording of simultaneous OH and CH_2O images with a high degree of temporal resolution can provide a better understanding of such turbulent flame phenomena as those of local extinction and of flame hole healing or re-ignition. CH_2O leakage through OH extinction points occurs more easily when there is a thin rather than a thick OH layer.

4.3.2 Simultaneous OH and acetone-PLIF

Since in a simultaneous OH and acetone experiment that was to be carried out, both OH and acetone could be excited by a 283 nm laser, only a single 283 nm laser was employed for excitation, the acetone serving as a fuel tracer. The acetone that was seeded was 8% by volume percentage of the total fuel that was pulsed into the jet flow by use of a bubbler. The experimental setup was the same in Figure 4.13 in section 4.3.1, except that the objects marked by an orange rectangular C were removed. The 355 nm laser (~160 mJ/pulse) went into action directly to pump the OPO, instead of splitting it into two beam paths.

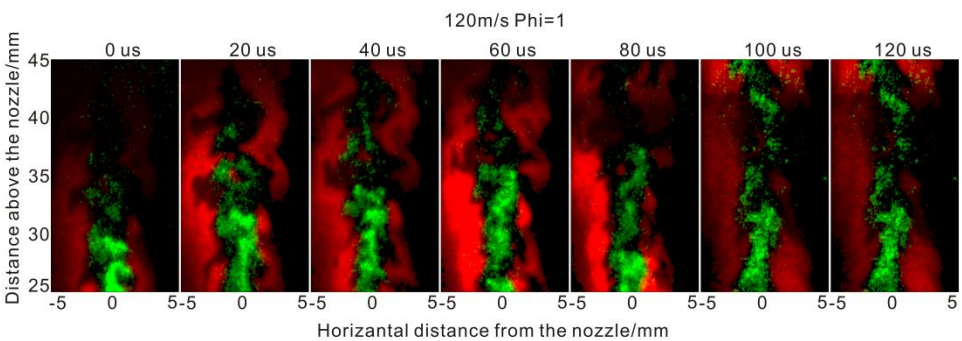

Figure 4.20 A time-resolved simultaneous sequence of OH (red) and acetone (green)-PLIF images.

Figure 4.20 shows a time resolved series of seven simultaneously captured OH-PLIF and Acetone-PLIF images of the turbulent premixed flame at a jet-flow speed of 120 m/s, where $\Phi = 1$. The data processing was the same as described in section 4.3.1, red indicating OH-PLIF and green indicating acetone-PLIF, respectively. The acetone-PLIF signal did not fill in the entire black area inside OH as CH_2O did. There was also no obvious acetone leakage through the OH quenching points in these images. Since the acetone was broken down first, intermediates such as formaldehyde formed before the temperature became high enough for OH to form.

4.4 OH and formaldehyde-PLIF by FRAME

A new versatile diagnostic method, termed the Frequency Recognition Algorithm for Multiple Exposures (FRAME), was presented here, one that enables instantaneous multiple species imaging to take place.

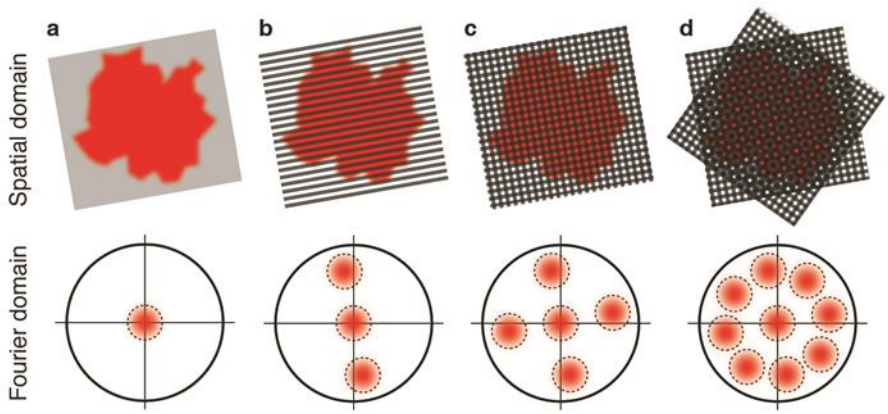

Figure 4.21 An illustration of the FRAME concept. (a) A uniformly illuminated sample, in which most of the sample structures are found near the center, at low spatial frequencies, of the Fourier domain. The outer circle marks the resolution limit of the detector. (b) Illuminating the sample with an intensity modulated pattern effectively places two 'copies' of the sample structures in otherwise unused space in the Fourier domain. (c)-(d) Each 'image copy' only fills a fraction of the available space, allowing multiple-illumination schemes without signal cross-talk.

The FRAME concept is illustrated in Figure 4.21 in which a coded field illuminates a sample that is characterized primarily by low spatial frequencies (i.e. weak gradients). Most of the sample information is thus condensed near the origin in the center of the Fourier domain (see Figure 4.21a) – the remaining space being mostly void. Image

copies of such a sample can thus be strategically placed at different locations in the vacant high frequency regions. If each modulation is unique (in terms of frequency and/or orientation), there will be an insignificant crosstalk between the copies, see d. Each copy fills only a fraction of the available space, allowing multiple-illumination schemes to appear without signal cross-talk.

The explanation of the FRAME algorithm is shown in Figure 4.22. A) A raw data video sequence, as seen by the camera and B) its Fourier transform. To access each frame individually, a 2D band-pass filter C), one having a super-Gaussian shape, is multiplied by the Fourier transform matrix, which temporarily removes the other image copies that are superimposed upon the photograph D). The filtered data is then transferred digitally to the center of the Fourier domain. F) taking the inverse Fourier transform of this data reveals the information which is stored at the offset location.

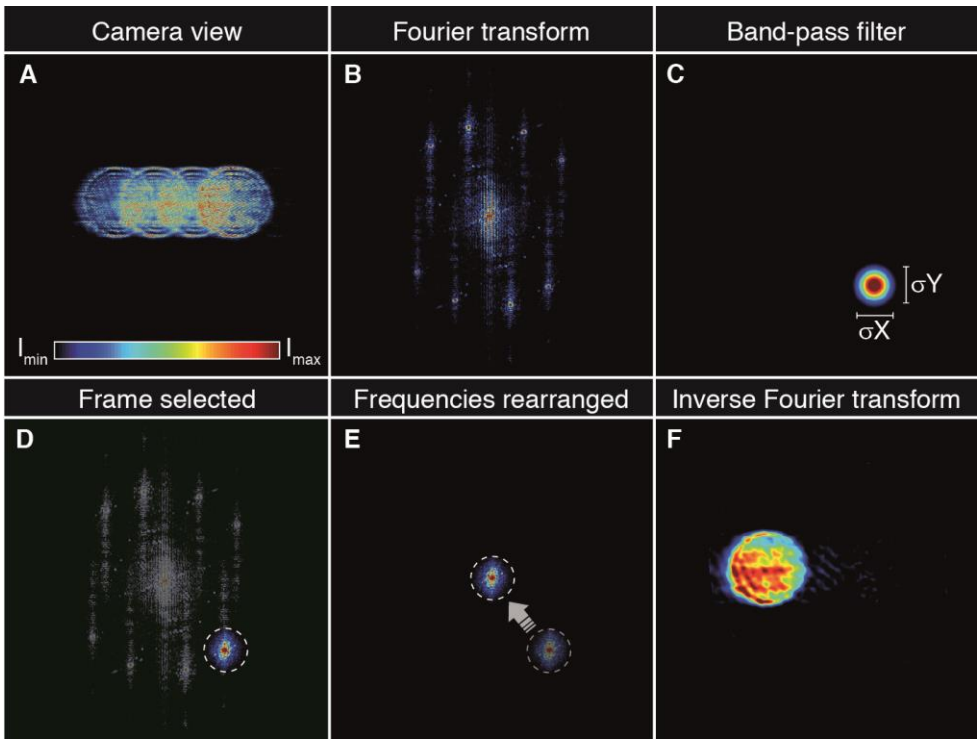

Figure 4.22 An explanation of the FRAME algorithm.

In the thesis work the FRAME concept has been employed taking ultra-high speed video (Paper A), in instantons 3D imaging (Paper B) and in simultaneous multi species imaging (Paper C).

4.5 Formaldehyde-PLIF through a borescope

Bowditch design optical engines have been employed for engine research since 1960s [24]. It is the most commonly used optical engine design used until now. However, it is not easy to employ the Bowditch design for the construction of large-bore ship engines, due to the large scale, the long stroke and the like involved. In this section, an attempt to make large-bore ship engine optically accessible is presented.

Instead of replacing the metal piston by quartz and putting quartz windows in the engine body, the researchers involved designed two optical inserts, which are so-called borescopes. The one insert was used for guiding the laser into the engine chamber and for reshaping the laser beam to form a thin laser sheet. The other insert was coupled with ICCD for signal detection purposes. This ship engine is a large-scale one that provides sufficient space for the two optical inserts involved. Figure 4.23 shows a sketch of the engine cover. In the engine there are two gas injectors and four pilot injectors. In contrast to passenger car or truck engines, this ship engine involved in the thesis work was using compressed air for starting up. In this study, the compressed air insert for starting was replaced by a laser insert, one of the pilot injectors being replaced by a detector insert, as indicated in Figure 4.23.

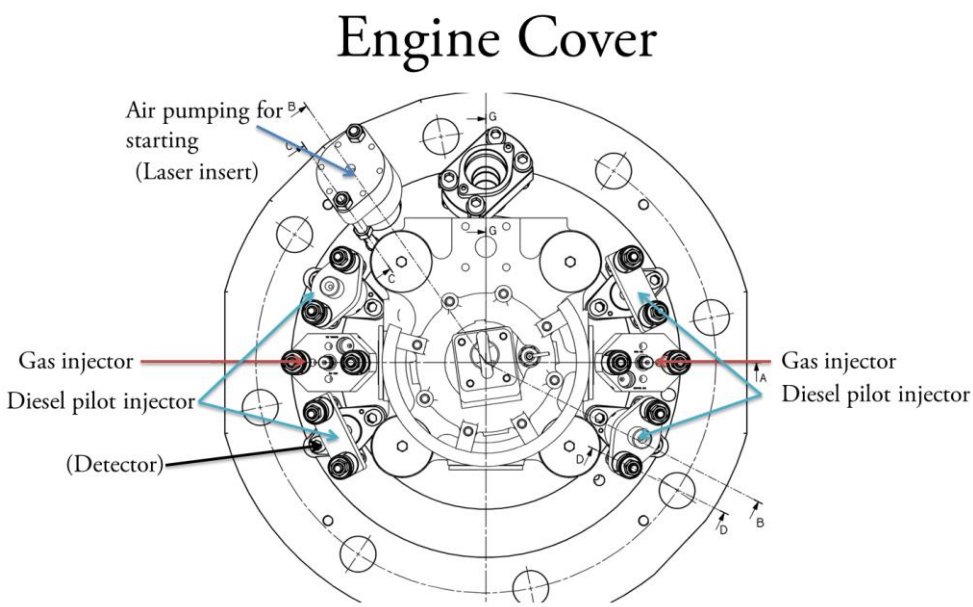

Figure 4.23 A sketch of the large bowl ship engine cover.

In the study, the gas fuel was ignited by diesel from the pilot injector. In order to investigate how the gas fuel ignites and burns, CH_2O-PLIF was planned to be employed. Figure 4.24 shows in 3D the relative position of the laser, the detector and the target fuel injector.

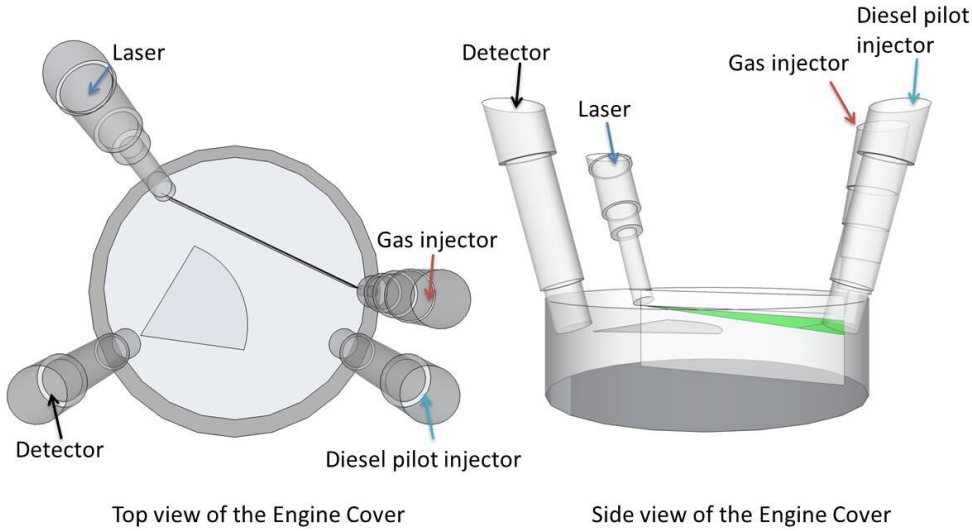

Figure 4.24 3D sketches of arrangement of the optical insert.

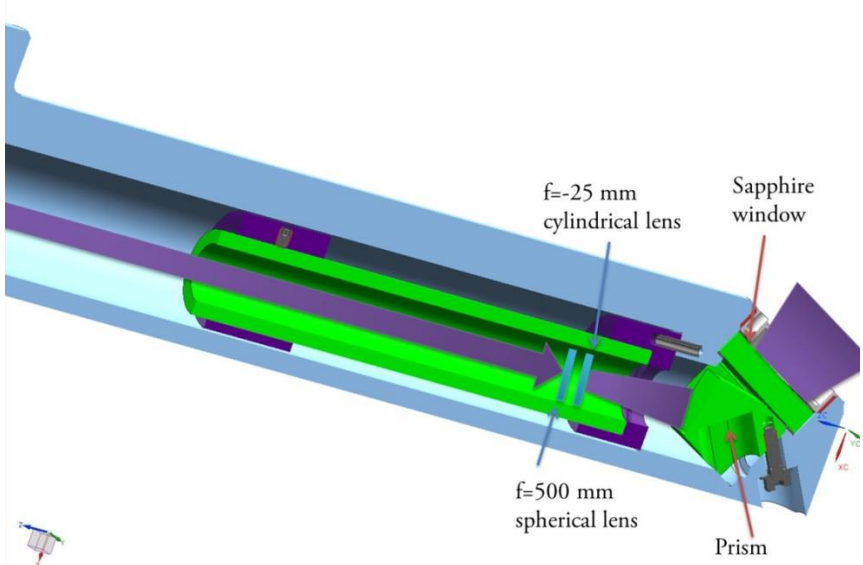

Figure 4.25 A sketch of the cross-section of the laser insert.

In this setup, the laser was aligned with the gas injector and the detector collected signals on the side toward the laser cross-section.

A sketch of the cross-section of the laser insert is shown in Figure 4.25. The input laser was a beam 6 mm in diameter, two reshaping lenses being placed in a tube as indicated in Figure 4.25. The inner diameter of the tube was 12.7 mm.

Unfortunately, due to machining errors, the sapphire window in the laser insert did not receive sufficient support from the metal surrounding it. It broke within a few cycles after the optically accessible cylinder started to move. Things were tried out three times. Each time, when the sapphire window broke, all of the optics in the tube were damaged. Thus, no CH_2O-PLIF images could be recorded during the investigation. However, the experience gained regarding these matters through this investigation being carried out is still valuable for the projects that will follow.

5 Experimental work - Soot optical diagnostics

Soot is one product of the hydrocarbon combustion process. It has proved to be harmful to human health [45]. The soot emissions of diesel IC engines are strictly regulated nowadays. The engine-out soot is considered to be the net result of the formation and oxidation of in-cylinder soot [46, 47]. Optical diagnostics has been introduced into the engine measurement of soot so as to be able to obtain a better understanding of the soot oxidation process. LEM [15, 48], measurements of the natural luminosity (NL) and LII [13, 49, 50] of flames are commonly employed for studying the soot in optical engines. The three techniques just referred to were all involved in the thesis work.

In this chapter, a short summary of Papers V through VII is provided. Additional results will also be presented in the discussion. Various challenges encountered in the experimental work and various suggestions are likewise discussed in the chapter.

5.1 Laser Extinction measurements

The fundamental principles involved in LEM are explained in section 3.5. The results for an optical engine achieved by use of LEM are employed in Paper V for analyzing soot oxidation. Conclusions regarding the effects there of the injection pressure, the diameter of injector nozzle and the level of the swirl of the engine could be drawn on the basis of the LEM data. A comparison was made of the results in Paper VI of LEM with those of flame natural luminosity. In the present section, various challenges encountered and considerations taken note of in the application of LEM to optical engines are discussed.

As mentioned in Paper V, the area of particular interest here was the recirculation zone between the two jets. One of the exhaust valves was replaced by an optical insert that provided laser access for the LEM measurements that were carried out. Figure 5.1 presents a schematic top view of the relative positions of the optical insert, the

optical piston and the probing laser there. The blue ring represents the rim of the quartz piston bowl. The orange dotted circle indicates where the window of optical insert was located. As can be seen, only a small part of the optical insert window permits the laser alignment that is marked by the grid. The optical insert is not perpendicular to the piston top but is tilted at an angle, a wedged quartz window being used to compensate for this insert tilting. The design is such that, if the probing laser is parallel to the axis of the optical insert, the laser passing through the wedged window should be perpendicular to the top of the piston. The fact that the area available on the insert is already quite limited resulted in various difficulties for proper alignment of the laser. The laser was checked regarding its being able to be held in the same position the whole time when the piston is moving up and down. It was also checked on each day prior to the measurements being made, that the laser was in the same position as on the last day on which measurements had been performed.

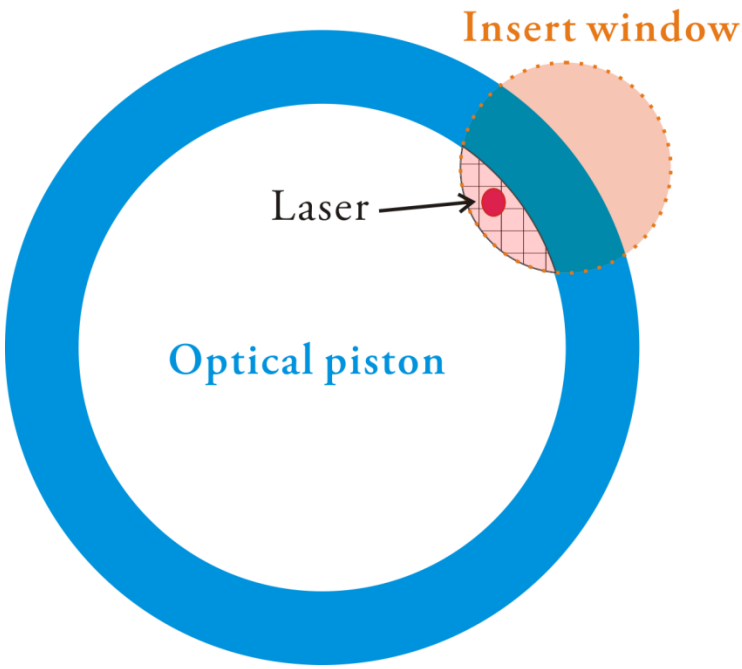

Figure 5.1 A schematic of the optical engine as seen from above.

An acousto-optic modulator (AOM) was used for intensity modulation of the laser beam. A schematic of the AOM, which consists of a piezoelectric transducer that creates sound waves in the quartz, is shown in Figure 5.2. A light beam is diffracted there into several orders. Through vibrating the quartz by use of a pure sinusoidal wave and tilting the AOM so that light would be reflected from the flat sound waves into the first order of diffraction, a deflection efficiency of up to 90% could be

achieved.[51] In the thesis work, the first order after AOM was selected for the LEM measurements that were carried out.

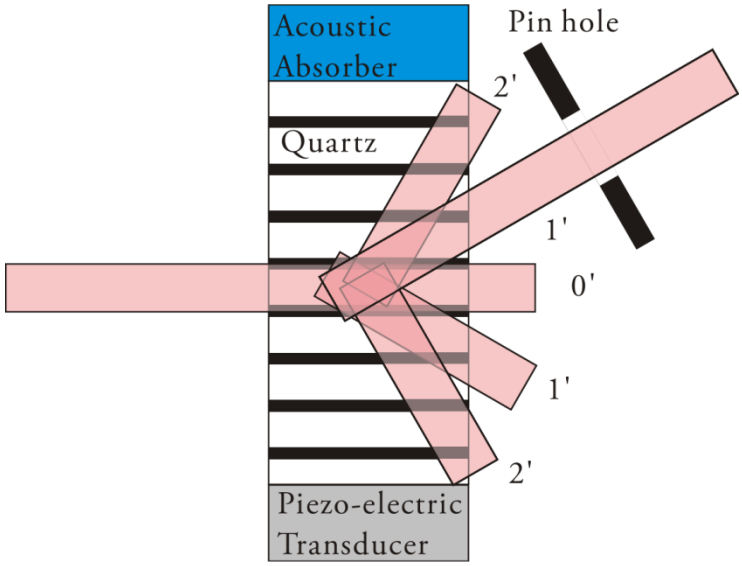

Figure 5.2 A schematic of the path of the laser through AOM.

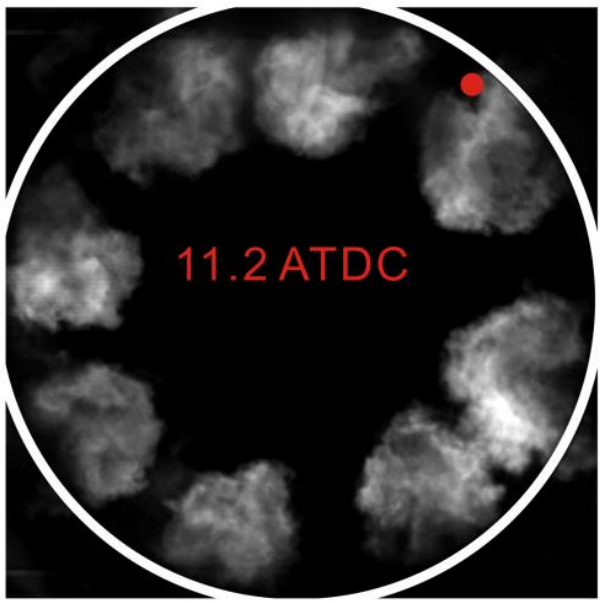

Figure 5.3 A natural luminosity image at 11.2 CAD as taken through the optical access. The white circle represents the wall of the piston bowl and the red dot represents the approximate position of the laser.

Figure 5.3 shows an image from a high speed video taken during the experiment. In the image, the natural luminosity of flame was recorded. The white circle represents the wall of the piston bowl and the red dot shows approximately the location of the laser during the experiments.

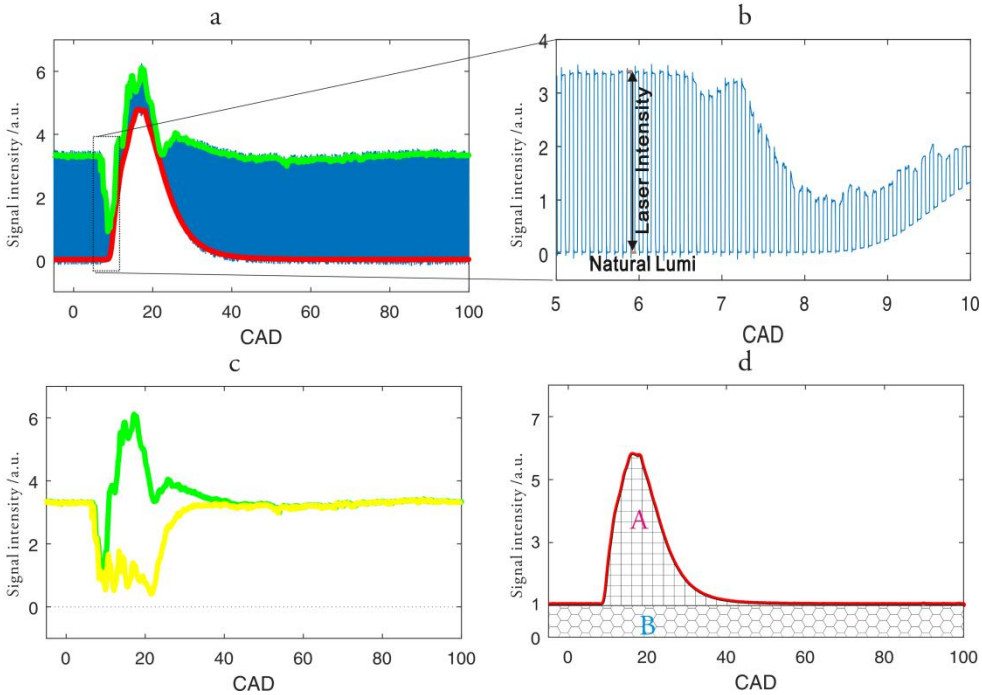

Figure 5.4 The raw intensity of the signal from the PD is plotted in a) as a function of CAD; b) presents an enlarged view of the plot in the rectangular marked section shown in a); the signal intensity when the laser is on is plotted in the green curve in c), the yellow curve there being the calculated laser intensity curve, and d) shows how a background luminosity curve would looked if a zero order laser diffraction were used.

Figure 5.4a) presents raw data collected from the photodiode (through transmission). Figure 5.4b), in turn, provides an enlarged view of the raw data within the range of 5 to 10 CAD, allowing the laser pulses to be identified, the amplitude of the modulation being calculated for each pulse. Both the laser transmission intensity for each laser pulse and the background luminosity can be obtained from the raw data on the basis of the mean top and mean bottom values. In Figure 5.4a) the mean top and bottom values are indicated by the green and the red curves, respectively.

In principle, a continuous laser can be employed for LEM measurement in cases in which the laser is the only signal source. The green curve in Figure 5.4c) shows the signal intensity of the photodiode when it a continuous wave laser was employed in

the optical engine. The background luminosity with use of a pulsed laser is shown as the red curve in Figure 5.4a). When the background luminosity is known, the laser intensity can be calculated through subtracting it from the total signal intensity. The yellow curve in Figure 5.4c) represents the calculated transmitted laser intensity. During the combustion process, the background luminosity of the flame is by no means negligible as compared with the laser intensity. Thus, pulsed lasers were involved in the thesis work.

The fact that the maximum deflection efficiency of AOM is 90% means that at least 10% of the input laser is delivered continuously at the zero order diffraction. The output of the zero order is a top-hat-shaped pulsed laser, yet the output intensity between two pulses is not zero. If one assumes that the graph of the background in Figure 5.4d) was collected with use of a probing laser from a laser of zero order diffraction, it can be seen that the red curve never returns to zero but has a constant offset of 1. However, the offset of zero order cannot be removed by simply subtracting a value of 1 from the red curve. In the graph, the red curve represents the sum of the flame luminosity and the continuous laser residual from the zero order laser diffraction. However, during the combustion process the residual of the continuous laser would also be absorbed by in-cylinder soot. Under such conditions, the background intensity calculated from Figure 5.4d) could not be related in an accurate manner to the natural luminosity of the flame. The zero order laser diffraction could be used in cases in which the background intensity was very strong that the continuous laser residual was negligible. In the thesis work one of the first order laser deflections from AOM was used for all the LEM measurements.

5.2 Comparison of LEM and NL

A comparison of the natural luminosity of the flame with the LEM was reported in Paper VI. A correction of the LEM data was performed to remove fluctuations in the laser intensity and soot deposition on the optical window. The corrected *KL* curve shows the low temperature soot that is found when NL is below the detection limit. The *KL* curve obtained from LEM was found to rise earlier than the corresponding NL curve did, due to interference caused by the diesel fuel spray. In this section, further results obtained under a variety of different engine conditions as well as certain additional results are presented.

In Figure 5.5 a plot of the *KL* factor for LEM and for NL, shown as a function of time, is presented. Three peaks can be identified in the *KL* curve, but only one main peak in the NL curve.

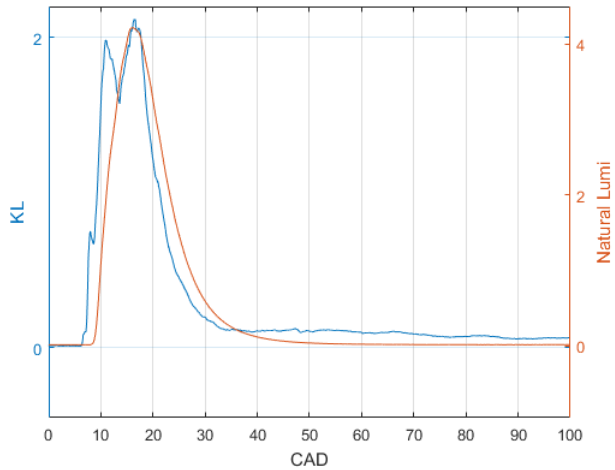

Figure 5.5 A *KL* and an NL curve shown as a function of CAD, replotted from Paper VI.

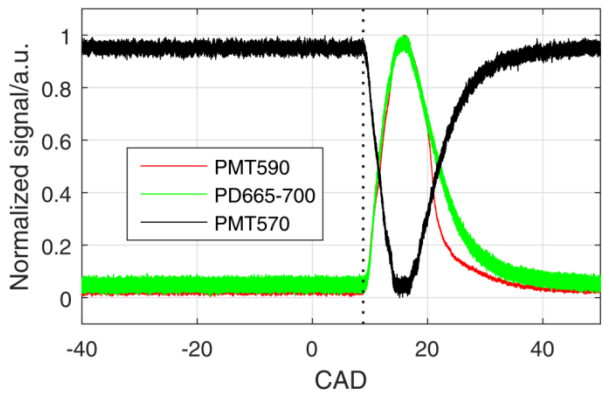

Figure 5.6 Normalized results for two PMTs and one photodiode, each differing in the filters employed.

In Paper VI, the authors explained the first peak on the *KL* curve as being due to the effects of the liquid fuel spray employed. The measurements were repeated several times and it was found that differences between the two curves could be observed consistently when engine conditions were basically the same in each case. Two photomultipliers (PMTs) were used for investigating whether there was any low-intensity signal from the natural luminosity of the flame too low to be detected by PD,. Figure 5.6 shows a normalized plot based on data recorded here from PMTs and PD. All of the data from the different detectors was recorded simultaneously. As can be seen, the degree of natural luminosity was detected by all three detectors at the

same time, as indicated by the dotted line. No low-intensity radiation was detected by the two PMTs before 8 CAD had been reached.

Such LEM and NL measurements were also carried out for another 12 engine conditions with use of the same fuel-injection pressure, except for the case discussed in Paper VI. The intake temperature, the density at TDC, and the engine RPM were varied during testing. A summary of the different engine conditions employed is presented in Table 5.1. The time from the start of injection to the rising of the *KL* and NL curves was calculated for each of the cases separately. The results are shown in the boxplot in Figure 5.7.

Table 5.1 Summary of the engine conditions.

Case No.	Density[kg/m^3]	T_{in}[K]	P_{inj}[bar]	RPM
1	19	1000	1500	1050
2	15.2	1000	1500	1050
3	17.1	1000	1500	1050
4	20.9	1000	1500	1050
5	22.8	1000	1500	1050
6	19	900	1500	1050
7	19	950	1500	1050
8	19	1050	1500	1050
9	19	1100	1500	1050
10	19	1000	1500	900
11	19	1000	1500	975
12	19	1000	1500	1125
13	19	1000	1500	1200

In Figure 5.7, it can be seen that the rising time of the *KL* curve varies very little between the different engine conditions employed, whereas the rising time of the NL curve changes from 1040 μs to 1560 μs. This indicates that the rising time of the *KL* curve is not affected significantly by the intake temperature, the top dead center density, or the engine RPM.

From early work by Naber et.al [52] on diesel spray penetration, it was known that the key parameter for estimating the fuel penetration time, from the injector to the

laser beam path, is the fuel velocity at the orifice, which is proportional to the square root of fuel pressure drop at the orifice [52]. Since the fuel pressure in the rail was semi-constant for all cases at 1500 bar, the in-cylinder peak pressure variation obtained was less than 10 bar, for the different engine cases, which is negligible as compared with the fuel pressure. Thus, the fuel pressure drop for the different cases was semi-constant. The fuel spray penetration time was also semi-constant for the cases listed in Table 5.1. This also supports the conclusion in Paper VI that the early rise in *KL* curve is due to the liquid fuel spray crossing the laser beam path. The start of combustion varies rather decidedly with different engine conditions, as can be seen from the large range of rising times of the NL curve that can be obtained.

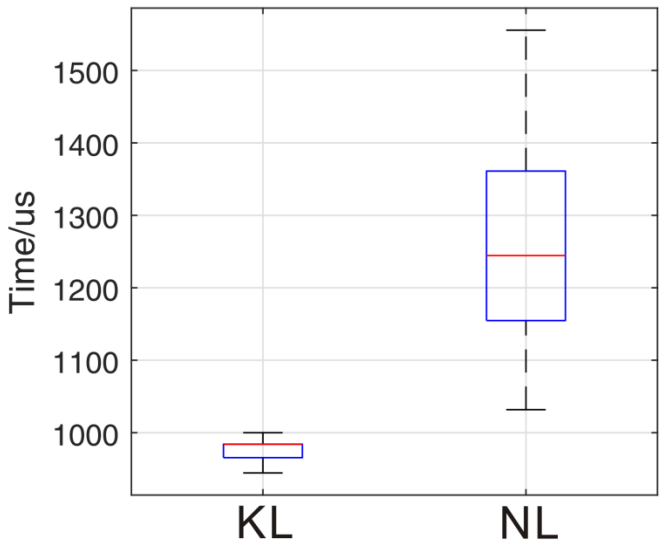

Figure 5.7 A boxplot of the time from the start of injection to the initial detection of *KL* and NL under the different engine conditions involved.

Figure 5.8 shows images of the natural luminosity of the flame as obtained by high-speed video. The video was taken without use of any optical filter, the detector not being UV/IR-sensitive. Soot luminosity is the main source of light in this video. The red dotted circle indicates the approximate location of the LEM probing laser beam. In Figure 5.5 one can see, in addition to the peak induced by the liquid fuel spray, another two peaks in the *KL* curve.

As can be seen in Figure 5.8, in the region in which the laser probing takes place the flame is not locally homogeneous, flame motion being introduced by the swirl that produces changes in the soot volume along the path of the laser beam. In the high-

speed video, this motion of the flame repeats itself to a considerable degree from cycle to cycle. Thus, more than one peak can be observed in the averaged *KL* curve.

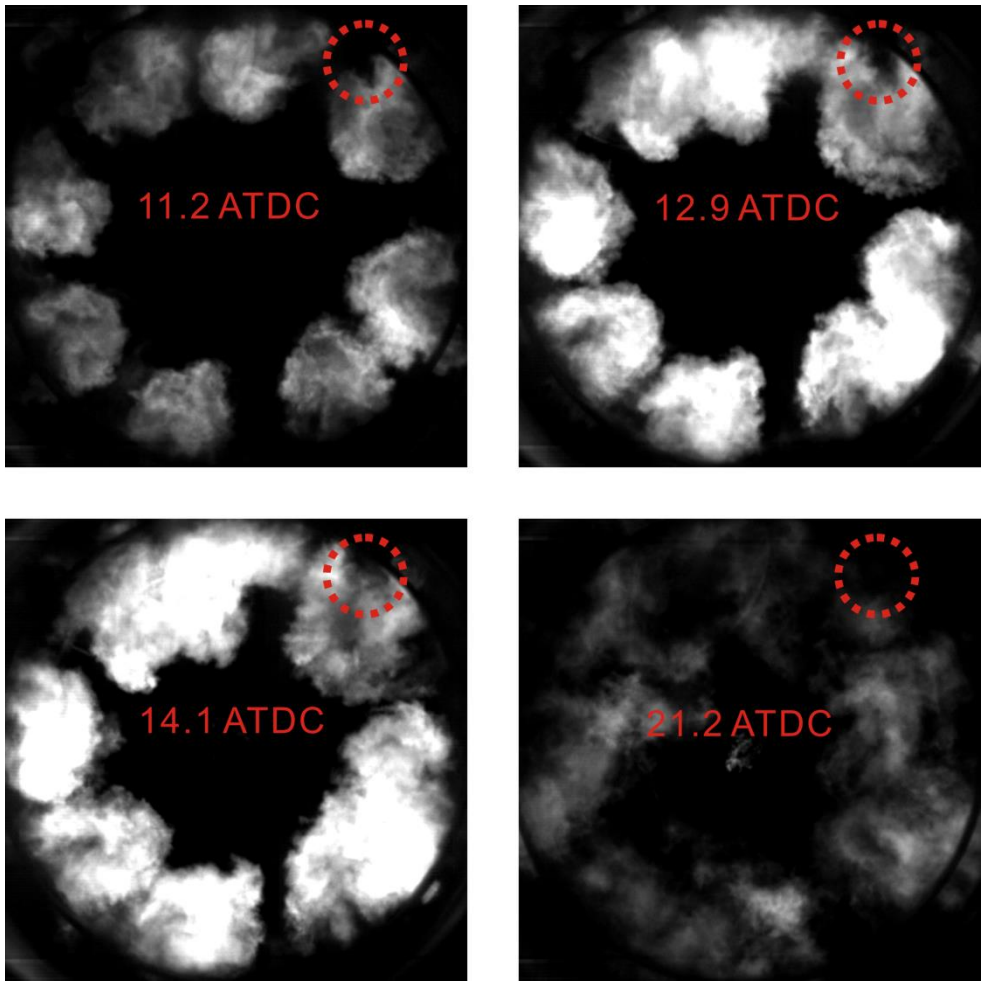

Figure 5.8 shows in a high-speed video the sequences of images produced by the natural luminosity of the flame. The red dotted circle indicates roughly the region in which the probing laser is located.

5.3 Soot-LII and OH-PLIF

Soot is one of the harmful products produced in hydrocarbon combustion, OH being the marker of the high-temperature reaction zone. It is believed that the OH involved needs to be readily available for the interaction with the soot in the oxidation process to take place. Even if a large amount of OH is formed, it may not lead to an effective oxidation process if it is not formed close to the bulk of the soot clouds. Simultaneous soot-LII and OH-PLIF imaging was employed in Paper VII for analyzing how the OH and the soot interact in the recirculation zone.

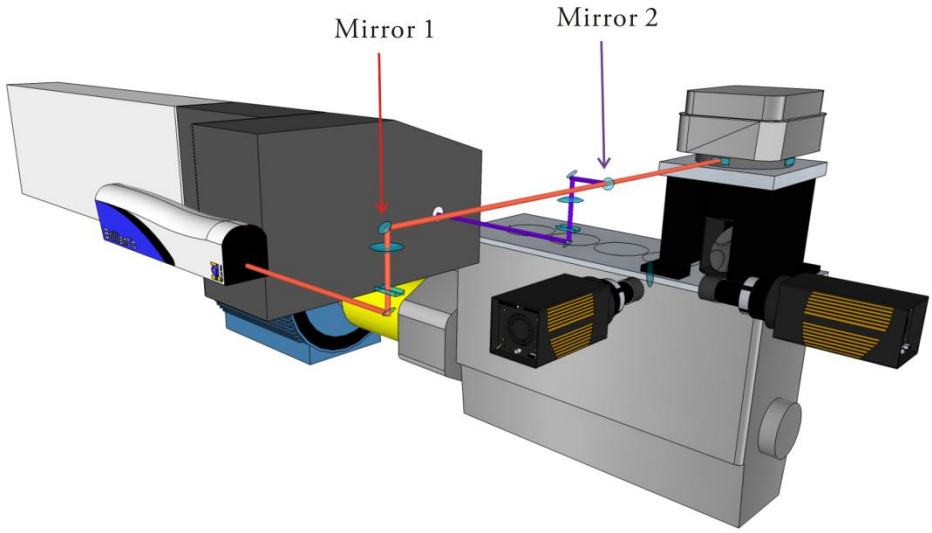

Figure 5.9 An overall view of the optical setup as replotted from Paper VII.

In the present work, 1064 nm laser was used for LII excitation and 284 nm laser for OH-PLIF excitation. Since the difference in wavelength between these two lasers is considerable, it is not recommended that one use the same optics in both cases for reshaping the laser beams. Figure 5.9 presents a sketch of the optical setup. Mirror 2 is a dichroic mirror that reflects 284 nm laser and lets 1064 nm laser pass. The beam forming optics for both lasers are mounted in front of mirror 2.

The beam-forming optics for the 1064 nm laser are placed in front of mirror 1. The reason for this is that during the experiments the location of the lasers may need to be moved up or down. In the current arrangement, it is only necessary to move the position of mirror 1 in order to increase or to lower the height of the 1064 nm laser beam.

As can be seen in Figure 5.9, the lasers were lifted in order to access the optical window in the engine. The lasers that were lifted were actually at about the height of human eyes. A careful shielding of the lasers is especially important to prevent injury in this case. The back reflection of the laser light from the optical liner in the engine needs to be tracked and thoroughly blocked.

The synchronization of this setup is shown in Figure 5.10. Since the power of the laser is much greater for the LII than for the LIF laser, the LII laser was triggered 1 μs later than the OH-PLIF laser was, so as to minimize the disturbance of the high power LII probing lasers. This is a sufficient delay to prevent any cross-talk of the LII signal with the short-lived OH-LIF signal.

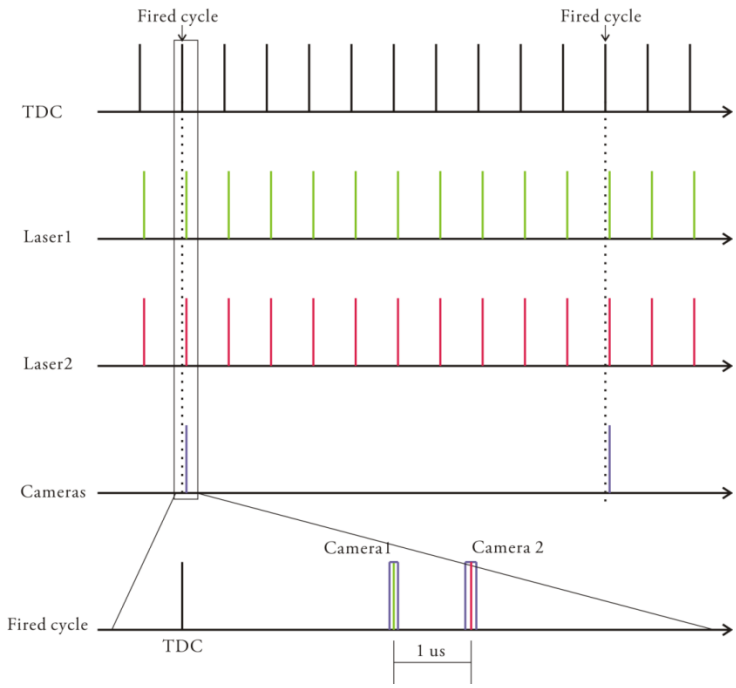

Figure 5.10 The synchronization scheme used for the optical measurements, as replotted from Paper VII.

When the engine was stabilized at 1200 rpm, both lasers were synchronized with the engine at 10 Hz by use of a 'phaser', the highest repetition rate of our ICCD cameras then being less than 5 Hz. Thus a 1 Hz pulse signal from the cycle that was fired was generated by the controlling program. The logical 'and-gate' was used for triggering the camera. The two inputs were a 10 Hz Q-switch out signal and 1 Hz fired cycle indicating pulse. This allows the camera to operate at 1 Hz and to be synchronized with the fired cycle.

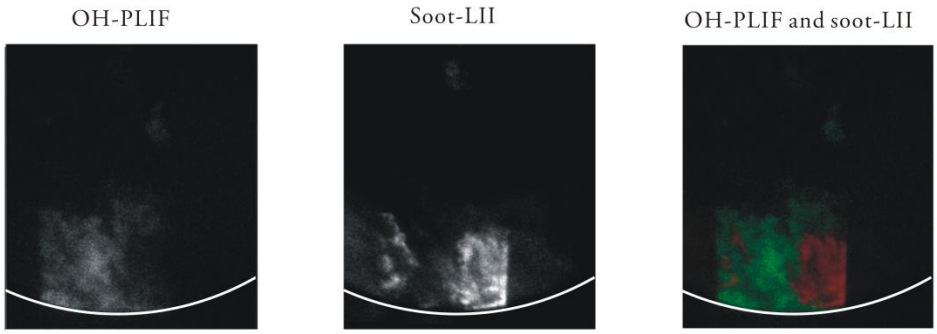

Figure 5.11 An example of two post processed images of OH and of soot. In the image to the right OH is colored green and soot red.

Figure 5.11 presents an example of a soot-LII image and an OH-PLIF image at 10 CAD that were both recorded simultaneously. The white curve indicates where the wall of the piston bowl is located. The superimposed image of the OH-PLIF and the soot-LII are located at the right. One can note that the shape of the OH cloud and that of the soot cloud fit very well with each other.

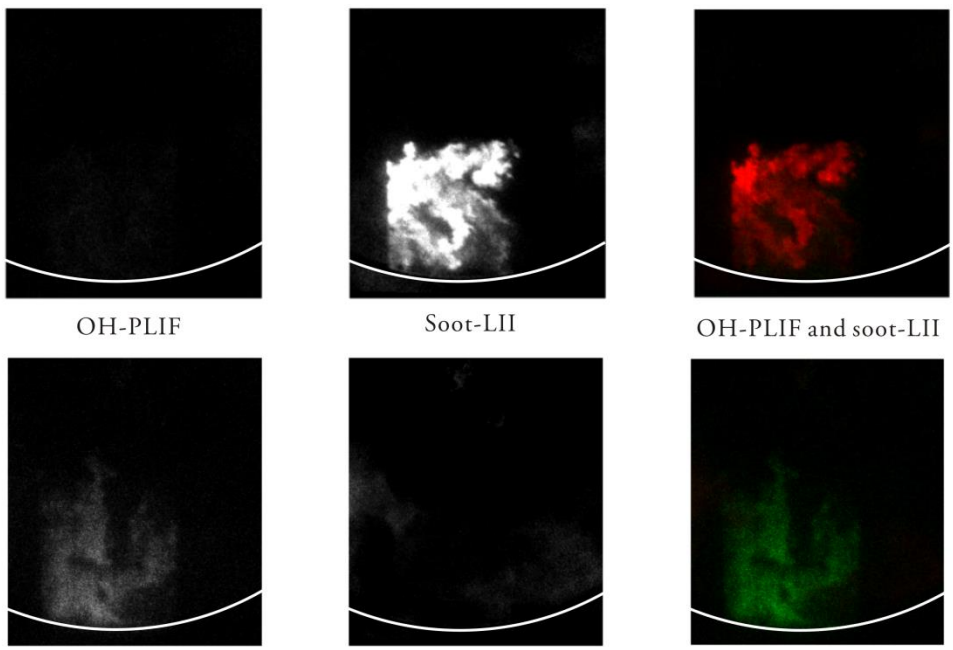

Figure 5.12 Results of various sorts obtained under differing engine conditions.

Figure 5.12 shows two examples involving two other engine cases, also recorded at 10 CAD. In this study the reason for the simultaneous imaging of both OH-PLIF and soot LII is to observe the interaction between the soot and the OH. The images in Figure 5.12, however, show only one useful distribution. By using the slope in the heat release trace caused by the late cycle oxidation one can, as suggested by Lequien et.al [47] determine a "half-life" of the late cycle oxidation. All the imaging was then done at the CA50+1.5 "half-lives" in Paper VII.

6 Summary and outlook

In summary, the thesis is concerned primarily with the development and application to optical engines of OH and soot optical diagnostics. Simultaneous dual species PLIF techniques are developed parallel to one another.

At the start, the online/offline OH* chemiluminescence method was used to hold the background luminosity in a sooty environment to a minimum, its helping to reduce part of the soot luminosity formed in the online image. For comparison purposes, the OH-LIF approach was used together with OH chemiluminescence imaging. It was found that the two methods yielded LOLs that were significantly different. The difference could be explained in terms of the 3D geometry effect.

LEM and LII were applied to an optical engine for obtaining soot measurements. A data correction of the preliminary LEM results was introduced so as to reduce the *KL* fluctuation obtained. The soot deposits on the optical window were also subtracted in the data correction carried out. OH-PLIF and soot-LII were employed simultaneously in analyzing the interaction between the soot and the OH in the late cycle. Problems in connection with fuel fluorescing, limited optical access, a harsh environment and signal synchronization were also addressed.

Simultaneously two species PLIF imaging – commonly used in connection with 10 Hz laser system – were extended through use of a laser having repetition rate of 50 kHz. Whereas for multi species imaging either more than one camera or a stereoscope is required, use of the FRAME approach enabled only a single camera to suffice dual species PLIF imaging. Each of these two imaging methods was demonstrated in the LUPJ burner.

Some suggestions for future work are provided in the followings.

Improving the signal-to-noise ratio in the FRAME images. The dual-species PLIF image quality in the FRAME work can be improved by use of better optics, i.e. quartz lenses and higher frequency quartz gratings. Simultaneous two species PLIF by use of FRAME was demonstrated. To the extent it is needed, simultaneous three or more species PLIF could be achieved by the FRAME approach.

Applying dual-species PLIF techniques to optical engines. Since both high speed and FRAME dual species have been demonstrated in a burner. Although it is more

challenging to apply them to optical engines than to the burner, it can be worthwhile to try this out. Use of dual-species data could also be promising for the study of partially pre-mixed combustion (PPC), e.g. for examining how well PPC occurs as compared with traditional diesel combustion or HCCI. The results are also of relevance to modelers for helping them improve their models.

High speed PLIF imaging of three or more species. Through adding a further camera or mounting a stereoscope on the framing camera, it is possible to do high speed OH, acetone and CH_2O-PLIF work with use of multi-YAG and OPO system. Various species other than OH can also be probed with use of such system, such as CH and CH_2O-PLIF.

High-speed quantitative PLIF. CMOS cameras coupled with a high speed intensifier is commonly are used for obtaining high-speed PLIF measurements. However, the use of high speed intensifier suffers from non linarites effects when a high repetition rate is employed. Since a framing CCD cameras has an individual intensifier for each CCD chips, non-linear effects do not appear with use of framing cameras. It is possible to obtain high-speed quantitative measurement with use of the multi-YAG and framing camera system, i.e. quantitative fuel tracer PLIF.

Double OPOs pumped by a single multi-YAG laser system. It is possible to split the laser power from multi-YAG so as to pump two OPOs separately, since in double-pulses mode multi-YAG can provide a power of 200 mJ/pulse, if the laser power is divided upon a 50/50 basis. In view of the conversion efficiency of BBO and KDP crystals the final output laser power could reach a level of about 1 mJ/pulse which is sufficient for many applications. With use of two OPOs, more potential species combinations can be probed simultaneously.

Acknowledgements

Several years ago, the acknowledgement part of my master thesis was evaluated as being the best one of all the theses ever published in the previous group. I hope that this time I will not get a similar comment. I hope one will pay more attention to the chapters prior to this part.

It was a fantastic time for me during the last four and half years that I have been working in this division. There are so many names I would like to mention but first of all, I am truly grateful to my supervisor, Professor *Mattias Richter,* for giving me the opportunity to work here. Having a strange Chinese student in the group must have been a tough decision for him. I really appreciate his guidance throughout all of my thesis work. Each time when I got stuck in the middle of a project, he always provided me the most valuable support possible and different practical solutions. His knowledge of engines and cars has made me feel really shameful as a man who earned both a master and a bachelor degree majoring in engines.

I would also like to thank my co-supervisor, Professor *Marcus Aldén,* for letting *Mattias* to bet on me and finance my work. I still remember our first meeting at Tianjin University. The efforts he had made for the whole division has inspired me a great deal.

Many thanks to Professor *Öivind Andersson* from the Combustion Engine Division. More than 70 percent of my thesis work was done with the collaboration of the Gendies group. There was lots of discussion at the Monday rig meetings. I would like to also thank Dr. *Guillaume Lequien, Ted Lind* and *Yann Gallo* for the long days we have been spent with one another in the lab.

Dr. *Elias Kristensson* is the most talented young researcher I've ever met. It was really my pleasure to work with him. I appreciate his sharing his brilliant ideas regarding the FRAME approach with me. We had many discussions about laser alignment and data processing. Thanks for listening to my often unpractical ideas.

I was so lucky to have shared the best student's office (at least I think so) in this Division with Dr. *Christoph Knappe* or *Dina Hot.* The first day I arrived in this Division, *Christoph* was the first person who spoke to me. I feel really sorry for him for always being so patient in listening to my complaints in the days that followed.

We had so much fun together both at work and after work. I knew *Dina* since she was a master student in this division. She is such a kind-hearted girl. She was always the first person I would like to ask a favor for. I believe I am not the only one in this Division who thinks in this way. I hope she can find a better office mate after I leave and the avocado tree will grow beyond the roof.

It was my honor to work in *Mattias'* group. Thanks to our previous colleagues Dr. *Johan Sjöholm,* Dr. *Johannes Lindén* and Dr. *Rikard Wellander*. I've learned a lot from them in the lab. I am also grateful to our current group members *Joakim Rosell, Fahed Abou Nada, Zhenkan Wang, Panagiota Stamatoglou* and *Alexios Matamis*. The trip to TU/e with them was unforgettable.

All my work has been done with the help of the whole division. Thanks to Professor *Per-Erik Bengtsson* and Dr. *Nils-Erik Olofsson* for their help on the OH-LIF and soot-LII project. Thanks to *Johan Simonsson* for his support to the LEM project. Thanks to *Jesper Borggren* for sharing his knowledge of TLAF with me. Thanks to Dr. *Edouard Berrocal* and Dr. *Andreas Ehn* not only for the enjoyable talks we have had in the middle of night in the Division, but also for sharing their great knowledge and experiences. Special thanks to *Minna Ramkull, Cecilia Bille* and *Igor Buzuk* for all the help you have given me during the last four and a half years.

I am grateful to *Johan Hult* in MAN Diesel & Turbo. It was really a nice experience working together with the industry. Thanks to Professor *Xue-Song Bai* from the Fluid Mechanics Division for sharing the knowledge of turbulent combustion with me.

I would like to take this opportunity to thank Dr. *Zhongshan Li* and Professor *Mingfa Yao*. I would not have been able to get here without your recommendations.

Thanks to Dr. *Bo Zhou,* Dr. *Jiajian Zhu,* Dr. *Yong He, Ye Zhang* and *Shufang Wei* for making otherwise boring weekends so joyful. Probably that is why I didn't miss China much when they were in Sweden, and the reason that I miss China so much now. Thanks to *Guillaume*, *Prakash, Slavey,* and whoever else from the Engine Division took part for those wonderful nights we've spent at pubs. Perhaps there were more people too associated with or the persons I've mentioned above who I should refer to as well but that a bit of alcohol may have meant that I am unable to recall our times together. Thanks to *Hadeel, Ulf, Ida* and *Ashish* for letting me have the opportunity to taste so many different delicious foods. Thanks to Dr. *Qiang Gao* and Dr. *Shuang Chen* for those parties full of alcohol and 'Chuiniubi'. I'm looking forward to meeting them in China and repeating the parties there. Special thanks to Dr. *Bo Li,* Dr. *Zhiwei Sun, Fan, Yajing, Xinming, Qing, Jinlong, Zhen, Siyuan, Chengdong, Jianfeng,* and *Wubin.*

I would like to thank the Competence Center for Combustion Processes (KCFP) and the China Scholarship Council (CSC) for their financial support.

Last but not least, I would like to thank my parents for all their supports. I am so lucky to have met *Mengqin Shen* in my life. We've been through all the joyful moments and tough periods together. I couldn't imagine what an idiot I would have been living somewhere in China if I hadn't met her. Thanks to *Matthew*, my dear, for making me forget all my troubles during a lovely hug or kiss.

References

[1] *Key world energy statistics 2015*. IEA. Online Available: http://www.iea.org/publications/freepublications/publication/KeyWorld_Statistics_2015.pdf

[2] *Energy and climate change*. IEA. Online Available: https://www.iea.org/publications/freepublications/publication/WEO2015SpecialReportonEnergyandClimateChange.pdf

[3] M. J. Dyer and D. R. Crosley, "Two-dimensional imaging of OH laser-induced fluorescence in a flame," *Optics Letters,* vol. 7, pp. 382-384, 1982/08/01 1982.

[4] C. F. Kaminski, J. Hult, and M. Aldén, "High repetition rate planar laser induced fluorescence of OH in a turbulent non-premixed flame," *Applied Physics B,* vol. 68, pp. 757-760, 1999/04/01 1999.

[5] J. Hult, U. Meier, W. Meier, A. Harvey, and C. F. Kaminski, "Experimental analysis of local flame extinction in a turbulent jet diffusion flame by high repetition 2-D laser techniques and multi-scalar measurements," *Proceedings of the Combustion Institute,* vol. 30, pp. 701-709, 1// 2005.

[6] A. Arnold, R. Bombach, B. Käppeli, and A. Schlegel, "Quantitative measurements of OH concentration fields by two-dimensional laser-induced fluorescence," *Applied Physics B,* vol. 64, pp. 579-583, 1997// 1997.

[7] J. Hult, A. Omrane, J. Nygren, C. Kaminski, B. Axelsson, R. Collin*, et al.*, "Quantitative three-dimensional imaging of soot volume fraction in turbulent non-premixed flames," *Experiments in Fluids,* vol. 33, pp. 265-269, 2002// 2002.

[8] I. Boxx, C. Slabaugh, P. Kutne, R. P. Lucht, and W. Meier, "3kHz PIV/OH-PLIF measurements in a gas turbine combustor at elevated pressure," *Proceedings of the Combustion Institute,* vol. 35, pp. 3793-3802, 2015.

[9] B. Peterson, E. Baum, B. Böhm, V. Sick, and A. Dreizler, "High-speed PIV and LIF imaging of temperature stratification in an internal combustion engine," *Proceedings of the Combustion Institute,* vol. 34, pp. 3653-3660, 2013.

[10] P. J. Trunk, I. Boxx, C. Heeger, W. Meier, B. Böhm, and A. Dreizler, "Premixed flame propagation in turbulent flow by means of stereoscopic PIV and dual-plane OH-PLIF at sustained kHz repetition rates," *Proceedings of the Combustion Institute,* vol. 34, pp. 3565-3572, // 2013.

[11] R. Wellander, M. Richter, and M. Aldén, "Time-resolved (kHz) 3D imaging of OH PLIF in a flame," *Experiments in Fluids,* vol. 55, 2014.

[12] A. W. Nicholas and R. D. James, "Tomographic reconstruction of OH* chemiluminescence in two interacting turbulent flames," *Measurement Science and Technology,* vol. 24, p. 024013, 2013.
[13] J. O'Connor and M. Musculus, "In-Cylinder Mechanisms of Soot Reduction by Close-Coupled Post-Injections as Revealed by Imaging of Soot Luminosity and Planar Laser-Induced Soot Incandescence in a Heavy-Duty Diesel Engine," *SAE Int. J. Engines,* vol. 7, pp. 673-693, 2014.
[14] K. Inagaki, S. Takasu, and K. Nakakita, "In-cylinder Quantitative Soot Concentration Measurement By Laser-Induced Incandescence," *SAE Technical Paper,* 1999-01-0508, 1999.
[15] M. P. B. Musculus and L. M. Pickett, "Diagnostic considerations for optical laser-extinction measurements of soot in high-pressure transient combustion environments," *Combustion and Flame,* vol. 141, pp. 371-391, 6// 2005.
[16] J. Hult, "Development of Time Resolved Laser Imaging Techniques for Studies of Turbulent Reacting Flows," Doctoral thesis, Department of Physics, Lund University, Lund, 2002.
[17] S. Johan, "High Repetition Rate Laser Diagnostics for Combustion Applications," Doctoral thesis, Department of Physics, Lund University, Lund, 2012.
[18] J. D. Miller, S. R. Engel, T. R. Meyer, T. Seeger, and A. Leipertz, "High-speed CH planar laser-induced fluorescence imaging using a multimode-pumped optical parametric oscillator," *Optics Letters,* vol. 36, pp. 3927-3929, 2011/10/01 2011.
[19] J. Sjöholm, E. Kristensson, M. Richter, M. Aldén, G. Göritz, and K. Knebel, "Ultra-high-speed pumping of an optical parametric oscillator (OPO) for high-speed laser-induced fluorescence measurements," *Measurement Science and Technology,* vol. 20, p. 025306, 2009.
[20] R. Wellander, "Multi-Dimensional Quantitative Laser-Based Diagnostics - Development and practial Applications," Doctoral thesis, Department of Physics, Lund University, Lund, 2014.
[21] B. Zhou, C. Brackmann, Z. Li, M. Aldén, and X.-S. Bai, "Simultaneous multi-species and temperature visualization of premixed flames in the distributed reaction zone regime," *Proceedings of the Combustion Institute,* vol. 35, pp. 1409-1416, // 2015.
[22] B. Zhou, "Advanced Laser-based Multi-scalar Imaging for Flame Structure Visualization Towards a Deepened Understanding of Premixed Turbulent Combustion," Doctoral thesis, Department of Physics, Lund University, 2015.
[23] B. Li, "Development and Application of Laser-Induced Emission Techniques for Combustion Diagnostics -High-Resolution Visualization of Turbulent Reacting Flows," Doctoral thesis, Department of Physics, Lund University, Lund, 2012.
[24] F. W. Bowditch, "A New Tool for Combustion Research A Quartz Piston Engine," *SAE Technical Paper 610002,* 1961.

[25] F. E. Belles and M. R. Lauver, "Origin of OH Chemiluminescence during the Induction Period of the H2–O2 Reaction behind Shock Waves," *The Journal of Chemical Physics,* vol. 40, pp. 415-422, 1964.

[26] B. Higgins and D. L. Siebers, "Measurement of the Flame Lift-Off Location on DI Diesel Sprays Using OH Chemiluminescence," *SAE Technical Paper,* 2001-01-0918, 2001.

[27] M. P. Musculus, J. E. Dec, and D. R. Tree, "Effects of Fuel Parameters and Diffusion Flame Lift-Off on Soot Formation in a Heavy-Duty DI Diesel Engine," *SAE Technical Paper,* 2002-01-0889, 2002.

[28] J. E. Dec and C. Espey, "Chemiluminescence Imaging of Autoignition in a DI Diesel Engine," *SAE Technical Paper,* 982685, 1998.

[29] A. C. Eckbreth, *Laser diagnostics for combustion temperature and species*: Gordon and Breach Publishers, 1996.

[30] J. Sjöholm, J. Rosell, B. Li, M. Richter, Z. Li, X.-S. Bai*, et al.*, "Simultaneous visualization of OH, CH, CH2O and toluene PLIF in a methane jet flame with varying degrees of turbulence," *Proceedings of the Combustion Institute,* vol. 34, pp. 1475-1482, // 2013.

[31] Z. S. Li, B. Li, Z. W. Sun, X. S. Bai, and M. Aldén, "Turbulence and combustion interaction: High resolution local flame front structure visualization using simultaneous single-shot PLIF imaging of CH, OH, and CH2O in a piloted premixed jet flame," *Combustion and Flame,* vol. 157, pp. 1087-1096, 6// 2010.

[32] C. Brackmann, J. Nygren, X. Bai, Z. Li, H. Bladh, B. Axelsson*, et al.*, "Laser-induced fluorescence of formaldehyde in combustion using third harmonic Nd:YAG laser excitation," *Spectrochimica Acta Part A: Molecular and Biomolecular Spectroscopy,* vol. 59, pp. 3347-3356, 12// 2003.

[33] L. A. Melton, "Soot diagnostics based on laser heating," *Applied Optics,* vol. 23, pp. 2201-2208, 1984/07/01 1984.

[34] K. H. Becker, D. Dley, and R. J. Norstrom, "OH* chemiluminescence in hydrocarbon atom flames," *Symposium (International) on Combustion,* vol. 12, pp. 405-413, 1969/01/01 1969.

[35] M. Aldén, H. Edner, and S. Svanberg, "Simultaneous, spatially resolved monitoring of C2 and OH in a C2H2/O2 flame using a diode array detector," *Applied Physics B,* vol. 29, pp. 93-97, 1982// 1982.

[36] J. E. Dec, "A conceptual Model of DI Diesel Combustion Based on Laser-Sheet Imaging," *SAE Technical Paper,* 970873, 1997.

[37] B. Higgins, D. L. Siebers, and A. Aradi, "Diesel-Spray Ignition and Premixed-Burn Behavior," *SAE Technical Paper,* 2000-01-0940, 2000.

[38] R. L. Gordon, A. R. Masri, and E. Mastorakos, "Simultaneous Rayleigh temperature, OH- and CH2O-LIF imaging of methane jets in a vitiated coflow," *Combustion and Flame,* vol. 155, pp. 181-195, 10// 2008.

[39] R. L. Gordon, I. Boxx, C. Carter, A. Dreizler, and W. Meier, "Lifted Diffusion Flame Stabilisation: Conditional Analysis of Multi-Parameter High-Repetition Rate Diagnostics at the Flame Base," *Flow, Turbulence and Combustion,* vol. 88, pp. 503-527, 2011.

[40] H. Zhao, *Advanced direct injection combustion engine technologies and development* vol. 2, 2010.

[41] S. Singh, Musculus, Mark P. B., Reitz, R.D., "Mixing and flame structures inferred from OH-PLIF for conventional and low-temperature diesel engine combustion," *Combustion and Flame,* vol. 156, pp. 1898-1908, 2009.

[42] M. P. B. Musculus, "Effects of the In-Cylinder Environment on Diffusion Flame Lift-Off in a DI Diesel Engine," *SAE Technical Paper,* 2003-01-0074, 2003.

[43] D. Siebers, Higgins, B. and Pickett, L., "Flame Lift-Off on Direct-Injection Diesel Fuel Jets: Oxygen Concentration Effects," *SAE Technical Paper,* 2002-01-0890, 2002.

[44] W. R. Hawthorne, D. S. Weddell, and H. C. Hottel, "Mixing and combustion in turbulent gas jets," *Symposium on Combustion and Flame, and Explosion Phenomena,* vol. 3, pp. 266-288, // 1948.

[45] M. Krzyzanowski, B. Kuna-Dibbert, and J. Schneider, *Health effects of transport-related air pollution*: WHO Regional Office Europe, 2005.

[46] U. Aronsson, C. Chartier, Ö. Andersson, R. Egnell, J. Sjöholm, M. Richter*, et al.*, "Analysis of the Correlation Between Engine-Out Particulates and Local Φ in the Lift-Off Region of a Heavy Duty Diesel Engine Using Raman Spectroscopy," *SAE Int. J. Fuels Lubr.,* vol. 2, pp. 645-660, 2009.

[47] G. Lequien, Ö. Andersson, P. Tunestal, and M. Lewander, "A Correlation Analysis of the Roles of Soot Formation and Oxidation in a Heavy-Duty Diesel Engine," *SAE Technical Paper,* 2013-01-2535, 2013.

[48] J. Manin, L. M. Pickett, and S. A. Skeen, "Two-Color Diffused Back-Illumination Imaging as a Diagnostic for Time-Resolved Soot Measurements in Reacting Sprays," *SAE Int. J. Engines,* vol. 6, pp. 1908-1921, 2013.

[49] G. K. Lilik, C. J. Mueller, C. E. Dumitrescu, and C. R. Gehrke, "The Visualization of Soot Late in the Diesel Combustion Process by Laser Induced Incandescence with a Vertical Laser Sheet," *SAE Int. J. Engines,* vol. 8, pp. 716-734, 2015.

[50] J. Sjöholm, R. Wellander, H. Bladh, M. Richter, P.-E. Bengtsson, M. Alden*, et al.*, "Challenges for In-Cylinder High-Speed Two-Dimensional Laser-Induced Incandescence Measurements of Soot," *SAE Int. J. Engines,* vol. 4, pp. 1607-1622, 2011.

[51] H. Eklund, A. Roos, and S. T. Eng, "Rotation of laser beam polarization in acousto-optic devices," *Optical and Quantum Electronics,* vol. 7, pp. 73-79, 1975// 1975.

[52] J. D. Naber and D. L. Siebers, "Effects of Gas Density and Vaporization on Penetration and Dispersion of Diesel Sprays," *SAE Technical Paper,* 960034, 1996.

Summary of papers

Paper I

Comparison of the Lift-Off Lengths Obtained by Simultaneous OH-LIF and OH* Chemiluminescence Imaging in an Optical Heavy-Duty Diesel Engine

Li, Z., Yu, X., Lequien, G., Lind, T., Jansons, M., Andersson, Ö. and Richter, M.

SAE Technical Paper 2015-24-2418, 2015, doi:10.4271/2015-24-2418.

I performed the experiment together with Guillaume Lequien and Ted Lind, I performed the image post-processing. Xin Yu and Marcis Jansons did the CFD simulation part. I was mainly responsible for writing the manuscript.

Paper II

Lift-Off Length in an Optical Heavy-Duty Diesel Engine

Lequien, G., **Li, Z.,** Andersson, Ö. and Richter, M.

SAE Int. J. Engines 8(2):635-646, 2015, doi:10.4271/2015-01-0793.

I performed the experiment together with Guillaume Lequien. We also cooperated in the data evaluation and preparing the manuscript for which Guillaume Lequien had the main responsibility for writing.

Paper III

Lift-Off Length in an Optical Heavy-Duty Diesel Engine: Effects of Swirl and Jet-Jet Interactions

Lequien, G., **Li, Z.,** Andersson, Ö. and Richter, M.

SAE Int. J. Engines 8(5):2188-2198, 2015, doi:10.4271/2015-24-2442.

I performed the experiment together with Guillaume Lequien. We also cooperated in the data evaluation and preparing the manuscript for which Guillaume Lequien had the main responsibility for writing.

Paper IV

Simultaneous imaging of dual species by Planar Laser Induced Fluorescence at 50 kHz in turbulent premixed flames

Li, Z., Rossel, J., Aldén, M. and Richter, M.

Submitted to Applied Spectroscopy

I performed the experiment together with Joakim Rossel. I designed and prepared the laser alignment with the help of Mattias Richter. I performed the image post-processing. I was mainly responsible for writing the manuscript.

Paper V

Parameters Influencing Soot Oxidation Rates in an Optical Diesel Engine

Gallo, Y., **Li, Z.,** Richter, M. and Andersson, Ö.

Accepted by SAE Powertrain Fuel and Lubricants 2016, 2016-01-2183

I performed the experiment together with Yann Gallo. I had the main responsibility for the laser diagnostics, while Yann was responsible for the engine rig. Yann was mainly responsible for the manuscript writing.

Paper VI

Comparison of laser-extinction and natural luminosity measurements for soot probing in diesel optical engines

Li, Z., Gallo, Y., Lind, T., Andersson, Ö., Aldén, M. and Richter, M.

Accepted by SAE Powertrain Fuel and Lubricants 2016, 2016-01-2159

I performed the experiment together with Yann Gallo. I had the main responsibility for the laser diagnostics, while Yann was responsible for the engine rig. I performed the data post-processing with the help of Mattias Richter. I was mainly responsible for writing the manuscript.

Paper VII

Simultaneous PLIF Imaging of OH and PLII Imaging of Soot for Studying the Late-Cycle Soot Oxidation in an Optical Heavy-Duty Diesel Engine

Lind, T., **Li, Z.,** Micó, C., Olofsson, N., Bengtsson, P.E., Richter, M. and Andersson, Ö.

SAE Int. J. Engines 9(2):2016, doi:10.4271/2016-01-0723.

I performed the experiment together with Ted Lind and Carlos Micó. Niles-Erik Olofsson and I had the main responsibility for the PLIF and the PLII laser setup, respectively, while Ted and Carlos were responsible for the engine rig. We also cooperated in the data evaluation and preparing the manuscript, for writing of which Ted Lind had the main responsibility.